Journal of Materials Chemistry C

Accepted Manuscript

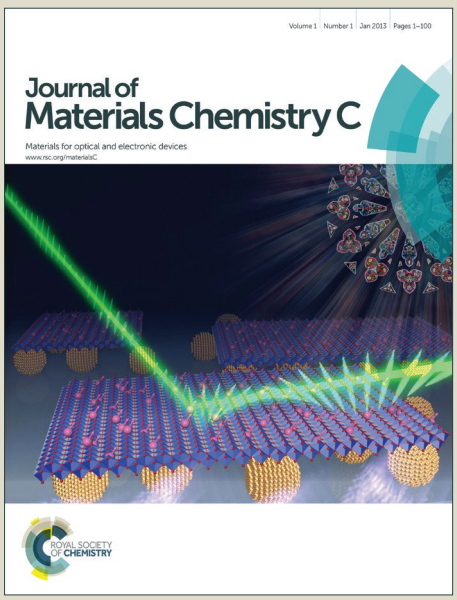

ROYAL SOCIETY OF CHEMISTRY

www.rsc.org/materialsC

Journal Name

ARTICLE

Solid State Red Biphotonic Excited Emission from Small Dipolar Fluorophores

Received 00th January 20xx,
Accepted 00th January 20xx

DOI: 10.1039/x0xx00000x

www.rsc.org/

Martin Ipuy,[a] Yuan-Yuan Liao,[a] Erwann Jeanneau,[b] Patrice L. Baldeck,[a] Yann Bretonnière,*[a] and Chantal Andraud*[a]

Dyes emitting in the solid state in the red or near-infrared range are much sought after for application in bioimaging especially if the long emission wavelentgh can be combined with two-photon excitation to provide unique contrast and penetration depth. In this article we present a series of small push-pull dipolar fluorophores based on 2-dicyanomethylene-3-cyano-4,5,5-trimethyl-2,5-dihydrofurane as electron accepting group. Compounds **1a**-**1m** differ only by the number (one, two or three) and the position of Methoxy groups on the electron-donor part. If these compounds are weakly emissive in dilute solution, they exhibit aggregation-induced emission properties and exciting solid state emission in the red - near infrared range very different from one compound to another highlighting the role of the number and of the position of the Methoxy electron-donor groups. The solid-state properties were studied by fluorescence spectroscopy and the solid state structure analyzed by X-ray diffraction showing that the presence of long chain of specific aggregates for the emitting species. Finally, the two-photon excitation properties were measured over the range 780-920 nm directly on the solid.

Introduction

Engineering of organic fluorophores emitting in the solid state has seen considerable development in the recent years thanks to practical applications in devices and optoelectronic materials such as organic light-emitting diodes (OLEDs)[1], solid-state lasers[2 3] or luminescent sensors,[4] and more recently in the field of bio-imaging in which they now represent a credible alternative to soluble fluorophores, particularly because of a markedly increased photostability.[5] In this last field, fluorophores with efficient red or near infra-red (NIR) emission are interesting for biological applications compared to yellow or green fluorescence.[5g, 6] Red emission can indeed lead to a great enhancement of detection thanks to a higher signal over noise ratio due to a lower scattering, a deeper light penetration and a better separation from medium auto-fluorescence. Moreover, combination with two-photon excitation provides additional advantages in term of imaging depth and resolution by shifting the excitation wavelength into the transparency window and exploiting the intrinsic confocal nature of two-photon excitation.

If two-photon excited fluorescence is now a well established technique for studying two-photon absorption properties of fluorophores in solution, reports of studies in the solid state are scarce although enhanced properties are expected in the aggregate state.[7] Most of them actually deal with colloidal suspension of nanoparticles [5i, 5j, 7-8] while direct measurement of two-photon absorption in crystal are even rarer.[9] Designing fluorophores that combined a solid-state emission in the red or NIR and efficient two-photon absorption properties is therefore of the highest interest representing a promising emerging field of research, and will be the subject of this article.

Red dyes are usually planar extended π-conjugated molecules or built along dipolar motif with donor (D) and acceptor (A) moieties.[1b, 10] This rigid structure helps to improve the fluorescence in dilute solution by reducing molecular rotations. It was believed that such geometry was responsible for weakly emissive fluorophores in densely aggregated state due to strong intermolecular π-π or dipole-dipole interactions. Several strategies have been validated to overcome the problem of fluorescence quenching due to aggregation. On one hand, introducing bulky groups at the periphery of the conventional highly fluorescent compounds such as perylene,[11] Nile Red,[12] Bodipy and boron-based derivatives,[13] or isolating the fluorophore in the core of a dendrimer [14] prevent close packing and restore the fluorescence in the solid-state. On the other hand, some peculiar molecules showing almost no fluorescence in dilute solution and usually based on polyaryl flexible systems such as tetraphenylethylenes (TPE), substituted stilbenes or siloles, become highly emissive when aggregated in the solid-state. This phenomenon, known as aggregation-induced emission

[a] Laboratoire de Chimie de l'ENS de Lyon, CNRS UMR 5182, ENS de Lyon, Université Lyon I. 46 allée d'Italie, 69364 Lyon cedex (France).
*E-mail: yann.bretonniere@ens-lyon.fr
[b] Centre de Diffractométrie Henri Longchambon, Université Lyon I. 43 boulevard du 11 Novembre 1918, 69622 Villeurbanne Cedex (France).

Electronic Supplementary Information (ESI) available: additional figures, characterizations and X-ray crystallographic data. See DOI: 10.1039/x0xx00000x

Chart 1 Structures of solid-state fluorescent TCF dyes **1a**-**1m**.

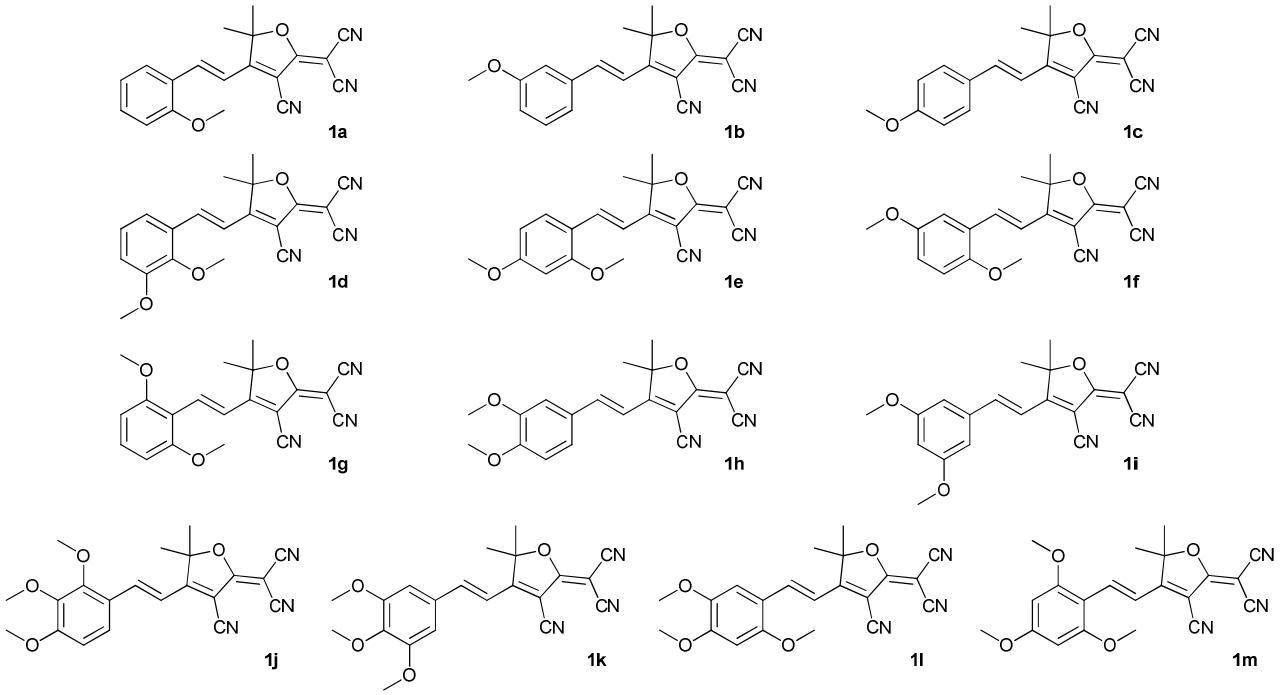

(AIE)[15] or aggregation-induced emission enhancement (AIEE)[16] has been proved to be related solely to the restriction of intramolecular movements (vibrational and rotational) in the aggregated state, the formation of particular type of aggregates in the solid only serving as effective way to rigidify the structure and restrict the intramolecular movements. AIE dyes therefore differentiate from conventional fluorophores and showed huge potential in many applications in the field of optics, electronic, energy storage and biomedicine and even forensic science.[17] Despite the tremendous synthetic work achieved for AIE/AIEE fluorophores, the rational design of new families of solid emitting fluorophores remains a challenge.

Yet, recent studies have also highlighted how subtle changes such as different side substituent or terminal functional groups can dramatically affect the crystal packing and, as a consequence, the solid-state emission.[16c, 18] However, relation between structure and aggregation remains unclear despite recent efforts to rationalize it [16c] and understanding the role of the self-assembly and the interactions between molecules in determining fluorescent properties remains a key point in the design of new solid-state emitters.[19] We and other previously reported [8b, 20] that small push-pull dipolar structures are interesting templates for solid-state emission. The molecular packing and the fluorescence properties can be easily tuned by varying the terminal functional groups, either on the donor or the acceptor end.[8b, 20b] With dicyanoisophorone as electron-accepting group for instance, emission above 700 nm could be obtained when *J*-aggregates in the form of inclined alignment of dipoles are present in the packing resulting in sharpening of the excitation and red-shift of the fluorescence.[20a] 2-dicyanomethylene-3-cyano-4,5,5-trimethyl-2,5-dihydrofurane (TCF) is another strong electron-withdrawing group that has been essentially used in the design of highly active nonlinear optical materials.[21] Although solid state emission was not reported, dipolar dyes incorporating the TCF ring have also proved to be of great interest for biological imaging, but mostly in combination with *N,N*-dialkylamino groups as electron-donating group.[22] Furthermore, TCF dyes containing other electron-donating groups such as hydroxyl (HO-TCF)[23] or methoxy (MeO-TCF)[24] groups have seldom been described despite showing interesting fluorescence properties such as high sensitivity to the environment, while being more photostable than their *N,N*-dialkylamino equivalents.[24b] Interestingly, a huge enhancement of fluorescence with an increase of viscosity attributed to restricted rotation around the dicyanomethylene group was demonstrated, foreshadowing good AIE properties.[24b]

In this article, we extend the molecular engineering around this structure and present a selection of small dipolar MeO-TCF dyes (**1a-m**, Chart 1) presenting intense solid-state fluorescence in the red up to 732 nm. Compounds **1a**-**1m** only vary by the number (one to three) and the position (*ortho*, *meta* or *para* to the electron accepting part) of the methoxy substituent around the phenyl ring leading to drastic modifications of the optical properties. Three of them only bear one methoxy group: in *ortho* (*o*-MeO-TCF, **1a**), *meta* (*m*-MeO-TCF, **1b**) and *para* position (*p*-MeO-TCF, **1c**) with respect to the TCF group. Six present two substituents: *2,3*-diMeO-TCF (**1d**), *2,4*-diMeO-TCF (**1e**), *2,5*-diMeO-TCF (**1f**), *2,6*-diMeO-TCF (**1g**), *3,4*-diMeO-TCF (**1h**) and *3,5*-diMeO-TCF (**1i**). The four final compounds are three-times substituted: *2,3,4*-triMeO-TCF (**1j**), *3,4,5-tri*MeO-TCF (**1k**), *2,4,5*-triMeO-TCF (**1l**) and 2,4,6-triMeO-TCF (**1m**). Interestingly, we show that the solid state

fluorescence can be two-photon excited, which is very promising for using these systems in biological applications.

Experimental

General

Commercially available materials were used as received from Sigma-Aldrich, Alfa and Acros. Analytical thin-layer chromatography (TLC) was carried out on Merck 60 F254 precoated silica gel plate (0.2 mm thickness). Visualization was performed using a UV lamp. Column chromatography was carried out using Merck silica gel 60 (35-70 µm). Microwave syntheses were conducted in 20 mL sealed tube on a Biotage Initiator 2.5 single-mode reactor using external IR temperature control. ^{1}H and ^{13}C NMR spectra were recorded at room temperature on a Bruker AC 500 spectrometer. ^{13}C NMR spectra were recorded with complete proton decoupling. Chemical shifts are reported in ppm from tetramethylsilane with the solvent resonance as internal standard. For proton, data are reported as follows: chemical shift, multiplicity (s = singlet, d = doublet, t = triplet, q = quartet, m = multiplet, b = broad), coupling constants in Hz. Infrared spectra (IR) were recorded on a FT-IR spectrophotometer and are reported as wavelength numbers (ν/cm^{-1} Low resolution mass spectra were taken on Agilent 6120 Quadrupole LC-MS System. High resolution mass spectrometry measurements and elemental analysis were performed at the Service Central d'Analyse du CNRS (Lyon, France). Melting points were recording on a calibrated Koffler bench.

General protocol for Knoevenagel reaction

The aldehyde **3a**-**m** (1 mmol) and **TCF** [25] (1.05 mmol, 210 mg) were dissolved in 10 mL of anhydrous ethanol in a 20 mL microwave vial. 2 drops of piperidine were added. The vial was sealed with a pressure septum and the mixture was irradiated by focused microwave at 100°C for 30 minutes by controlling the temperature. After cooling, the precipitate was filtered and washed with ethanol to give the desired product that was purified by chromatography on silica gel eluting with CH_2Cl_2.

Synthesis and characterization

(E)-2-(3-cyano-4-(2-methoxystyryl)-5,5-dimethylfuran-2(5H)-ylidene)malono-nitrile (1a). From 2-methoxybenzaldehyde **3a** (136 mg) following the general procedure. Orange solid (144 mg, yield=45 %). ^{1}H NMR (DMSO-d6, 500 MHz, δ/ppm) 8.22 (d, 1 H, *J* = 16.4 Hz), 7.95 (d, 1 H, *J* = 8.0 Hz), 7.55 (t, 1 H, *J* = 8.0 Hz), 7.33 (d, 1 H, *J* = 16.4 Hz), 7.17 (d, 1 H, *J* = 8.0 Hz), 7.08 (t, 1 H, *J* = 8.0 Hz), 3.92 (s, 3 H), 1.76 (s, 6 H, -CH_3); ^{13}C NMR (DMSO-d6, 125 MHz, δ/ppm) 177.9, 176.4, 159.5, 143.0, 134.8, 130.6, 123.3, 121.6, 116.3, 113.3, 112.8, 112.5, 111.8, 99.9, 98.6, 56.7, 54.7, 25.5 (2 C); IR (ν/cm^{-1}) 3001, 2934, 2834, 2223, 1556, 1527, 1483, 1375, 1245, 757; Anal. calcd for $C_{19}H_{15}N_3O_2$: C 71.91, H 4.76, N 13.24; found: C 72.24, H 4.77, N 13.53; MS (ES$^-$, m/z): 318.0 (100 %), 378.9 (29.2 %) for $[M+H]^+$, 340.0 (26.8 %) for $[M+Na]^+$; m.p. > 260°C.

(*E*)-2-(3-cyano-4-(3-methoxystyryl)-5,5-dimethylfuran-2(5*H*)-ylidene)malono-nitrile (1b). From 3-methoxybenzaldehyde **3b** (136 mg) following the general procedure. Orange solid (190 mg, yield=60 %). ^{1}H NMR (DMSO-d6, 500 MHz, δ/ppm) 7.90 (d, 1 H, *J* = 16.4 Hz), 7.48 (d, 1 H, *J* = 8.4 Hz), 7.47 (s, 1 H), 7.43 (t, 1 H, *J* = 8.4 Hz), 7.23 (d, 1 H, *J* = 16.4 Hz), 7.11 (d, 1 H, *J* = 8.4 Hz), 3.84 (s, 3 H), 1.80 (s, 6 H, -CH_3); ^{13}C NMR (DMSO-d6, 125 MHz, δ/ppm) 177.7, 175.7, 160.3, 147.7, 136.3, 130.9, 122.3, 118.9, 116.3, 114.7, 113.2, 112.4, 111.4, 100.3, 100.1, 56.0, 55.2, 25.6 (2 C); IR (ν/cm^{-1}) 2986, 2934, 2228, 1577, 1537, 1272, 829; Anal. calcd for $C_{19}H_{15}N_3O_2$: C 71.91, H 4.76, N 13.24; found: C 71.56, H 4.70, N 13.15 MS (ES$^-$, m/z): 318.0 (100 %), 378.9 (24.7 %) for $[M+H]^+$, 340.0 (19.7 %) for $[M+Na]^+$; m.p. > 260°C.

(*E*)-2-(3-cyano-4-(4-methoxystyryl)-5,5-dimethylfuran-2(5*H*)-ylidene)malono-nitrile (1c). From 4-methoxybenzaldehyde **3c** (136 mg) following the general procedure. Orange-red solid (172 mg, yield=54 %). ^{1}H NMR (DMSO-d6, 500 MHz, δ/ppm) 7.92 (d, 1 H, *J* = 16.4 Hz), 7.91 (d, 2 H, *J* = 8.4 Hz), 7.10 (d, 1 H, *J* = 16.4 Hz), 7.09 (d, 2 H, *J* = 8.4 Hz), 3.86 (s, 3 H), 1.79 (s, 6 H); ^{13}C NMR (DMSO-d6, 125 MHz, δ/ppm) 177.8, 176.3, 163.6, 148.3, 132.5 (2 C), 127.7, 115.5 (2 C), 113.4, 112.6, 111.7, 99.8, 98.1, 56.3, 54.2, 25.8 (2 C); IR (ν/cm^{-1}) 2986, 2960, 2897, 2212, 1580, 1563, 1249, 1165, 832; Anal. calcd for $C_{19}H_{15}N_3O_2$: C 71.91, H 4.76, N 13.24; found: C 71.85, H 4.68, N 13.31; MS (ES$^-$, m/z): 318.0 (100 %), 378.9 (26.4 %) for $[M+H]^+$, 340.0 (28.2 %) for $[M+Na]^+$; m.p. > 260°C.

(*E*)-2-(3-cyano-4-(2,3-dimethoxystyryl)-5,5-dimethylfuran-2(5*H*)-ylidene)malono-nitrile (1d). From 2,3-dimethoxybenzaldehyde **3d** (166 mg) following the general procedure. Yellow solid (217 mg, yield=62 %). ^{1}H NMR (DMSO-d6, 500 MHz, δ/ppm) 8.28 (d, 1 H, *J* = 16.4 Hz), 7.60 (d, 1 H, *J* = 7.4 Hz), 7.27 (d, 1 H, *J* = 16.4 Hz), 7.24 (d, 1 H, *J* = 7.4 Hz), 7.21 (t, 1 H, *J* = 7.4 Hz), 3.84 (s, 3 H), 3.81 (s, 3 H), 1.73 (s, 6 H, -CH_3); ^{13}C NMR (DMSO-d6, 125 MHz, δ/ppm) 178.0, 176.1, 153.4, 149.3, 142.0, 128.4, 125.2, 120.1, 117.2, 116.8, 113.2, 112.4, 112.0, 100.0, 98.7, 61.8, 56.5, 55.0, 25.2 (2 C); IR (ν/cm^{-1}) 2981, 2970, 2902, 2225, 1567, 1536, 1272, 1105, 990; Anal. calcd for $C_{20}H_{17}N_3O_3$: C 69.15, H 4.93, N 12.10; found: C 69.37, H 4.91, N 12.12; MS (ES$^-$, m/z): 346.0 (100 %), 347.1 (24.5 %) for $[M-H]^-$; m.p. > 260°C.

(*E*)-2-(3-cyano-4-(2,3-dimethoxystyryl)-5,5-dimethylfuran-2(5*H*)-ylidene)malono-nitrile (1d). From 2,3-dimethoxybenzaldehyde **3d** (166 mg) following the general procedure. Yellow solid (217 mg, yield=62 %). ^{1}H NMR (DMSO-d6, 500 MHz, δ/ppm) 8.28 (d, 1 H, *J* = 16.4 Hz), 7.60 (d, 1 H, *J* = 7.4 Hz), 7.27 (d, 1 H, *J* = 16.4 Hz), 7.24 (d, 1 H, *J* = 7.4 Hz), 7.21 (t, 1 H, *J* = 7.4 Hz), 3.84 (s, 3 H), 3.81 (s, 3 H), 1.73 (s, 6 H, -CH_3); ^{13}C NMR (DMSO-d6, 125 MHz, δ/ppm) 178.0, 176.1, 153.4, 149.3, 142.0, 128.4, 125.2, 120.1, 117.2, 116.8, 113.2, 112.4, 112.0, 100.0, 98.7, 61.8, 56.5, 55.0, 25.2 (2 C); IR (ν/cm^{-1}) 2981, 2970, 2902, 2225, 1567, 1536, 1272, 1105, 990; Anal. calcd for $C_{20}H_{17}N_3O_3$: C 69.15, H 4.93, N 12.10; found: C 69.37, H 4.91, N 12.12; MS (ES$^-$, m/z): 346.0 (100 %), 347.1 (24.5 %) for $[M-H]^-$; m.p. > 260°C.

(*E*)-2-(3-cyano-4-(2,4-dimethoxystyryl)-5,5-dimethylfuran-2(5*H*)-ylidene)malono-nitrile (1e). From 2,4-dimethoxybenzaldehyde **3e** (166 mg) following the general procedure. Red solid (183 mg, yield=53 %). ^{1}H NMR (DMSO-d6, 500 MHz, δ/ppm) 8.18 (d, 1 H, *J* = 16.4 Hz), 7.93 (d, 1 H, *J* = 8.4 Hz), 7.21 (d, 1 H, *J* = 16.4 Hz), 6.70 (d, 1 H, *J* = 8.4 Hz), 6.69 (s, 1 H), 3.93 (s, 3 H), 3.89 (s, 3 H), 1.74 (s, 6 H, -CH_3); ^{13}C NMR (DMSO-d6, 125 MHz, δ/ppm) 178.0, 177.0, 165.7, 161.9, 143.9, 132.9, 116.7, 113.6, 113.4, 112.7, 112.1, 108.1, 99.4, 99.0, 96.1, 56.9, 56.5, 53.5, 25.8 (2 C); IR (ν/cm^{-1}) 3023, 2944, 2850, 2224, 1611, 1516, 1427, 1375, 1256, 1206; Anal. calcd for $C_{20}H_{17}N_3O_3$: C 69.15, H 4.93, N 12.10; found: C 68.84, H 4.89, N 11.81; MS (ES$^-$, m/z): 346.1 (100 %), 347.0 (29.9 %) for [M-H]$^-$; m.p. > 260°C.

(*E*)-2-(3-cyano-4-(2,5-dimethoxystyryl)-5,5-dimethylfuran-2(5*H*-)ylidene)malono-nitrile (1f). From 2,5-dimethoxybenzaldehyde **3f** (166 mg) following the general procedure. Brown solid (275 mg, yield=79 %). ^{1}H NMR (in DMSO-d6, 500 MHz, δ/ppm) 8.22 (d, 1 H, *J* = 16.4 Hz), 7.52 (d, 1 H, *J* = 4.2 Hz), 7.35 (d, 1 H, *J* = 16.4 Hz), 7.14 (dd, 1 H, *J* = 8.4 Hz, *J* = 4.2 Hz), 7.11 (d, 1 H, *J* = 8.4 Hz), 3.86 (s, 3 H), 3.79 (s, 3 H), 1.76 (s, 6 H, -CH_3); ^{13}C NMR (DMSO-d6, 125 MHz, δ/ppm) 178.0, 176.4, 154.2, 154.0, 142.9, 123.8, 120.9, 116.6, 114.4, 114.0, 113.3, 112.5, 111.8, 99.9, 98.5, 57.0, 56.4, 54.7, 25.5 (2 C); IR (ν/cm^{-1}) 3080, 2986, 2938, 2834, 2226, 1606, 1567, 1523, 1247, 1227; Anal. calcd for $C_{20}H_{17}N_3O_3$: C 69.15, H 4.93, N 12.10; found: C 69.48, H 4.89, N 12.30; MS (ES$^-$, m/z): 346.0 (100 %), 347.0 (20.6 %) for [M-H]$^-$; m.p. > 260°C.

(*E*)-2-(3-cyano-4-(2,6-dimethoxystyryl)-5,5-dimethylfuran-2(5*H*)-ylidene)malono-nitrile. (1g). From 2,6-dimethoxybenzaldehyde **3g** (166 mg) following the general procedure. Orange solid (263 mg, yield=76 %). ^{1}H NMR (DMSO-d6, 500 MHz, δ/ppm) 8.17 (d, 1 H, *J* = 16.4 Hz), 7.52 (d, 1 H, *J* = 8.4 Hz), 7.51 (d, 1 H, *J* = 16.4 Hz), 6.79 (d, 2 H, *J* = 8.4 Hz), 3.92 (s, 6 H, -OMe), 1.75 (s, 6 H, -CH_3); ^{13}C NMR (DMSO-d6, 125 MHz, δ/ppm) 177.8, 177.6, 161.1 (2 C), 139.6, 135.6, 117.9, 113.3, 112.6, 112.1, 111.7, 105.0 (2 C), 99.3, 98.2, 57.0 (2 C), 52.6, 26.1 (2 C); IR (ν/cm^{-1}) 2992, 2968, 2908, 2226, 1577, 1559, 1405, 1378, 1252, 1055; Anal. calcd for $C_{20}H_{17}N_3O_3$: C 69.15, H 4.93, N 12.10; found: C 69.28, H 4.66, N 12.03; MS (ES$^-$, m/z): 346.0 (100 %), 347.1 (30.3 %) for [M-H]$^-$; m.p. > 260°C.

(*E*)-2-(3-cyano-4-(3,4-dimethoxystyryl)-5,5-dimethylfuran-2(5*H*)-ylidene)malono-nitrile (1h). From 3,4-dimethoxybenzaldehyde **3h** (166 mg) following the general procedure. Red solid (163 mg, yield=47 %). ^{1}H NMR (DMSO-d6, 500 MHz, δ/ppm) 7.91 (d, 1 H, *J* = 16.4 Hz), 7.54 (d, 1 H, *J* = 8.4 Hz), 7.52 (s, 1 H), 7.11 (d, 1 H, *J* = 16.4 Hz), 7.11(d, 1 H, *J* = 8.4 Hz), 3.86 (s, 6 H), 1.80 (s, 6 H, -CH_3); ^{13}C NMR (DMSO-d6, 125 MHz, δ/ppm) 177.9, 176.2, 153.6, 149.8, 148.8, 127.9, 125.9, 113.5 (2 C), 112.6, 112.4, 112.0, 111.7, 99.7, 97.8, 56.4, 56.4, 54.1, 25.8 (2 C); IR (ν/cm^{-1}) 2987, 2971, 2901, 2226, 1556, 1521, 1406, 1379, 1257, 1069; Anal. calcd for $C_{20}H_{17}N_3O_3$: C 69.15, H 4.93, N 12.10; found: C 69.45, H 4.89, N 12.22. MS (ES$^-$, m/z): 346.0 (100 %), 346.9 (28.2 %) for [M-H]$^-$; m.p. > 260°C.

(*E*)-2-(3-cyano-4-(3,5-dimethoxystyryl)-5,5-dimethylfuran-2(5*H*)-ylidene)malono-nitrile (1i). From 3,5-dimethoxybenzaldehyde **3i** (166 mg) following the general procedure. Yellow solid (149 mg, yield=42 %). ^{1}H NMR (DMSO-d6, 500 MHz, δ/ppm) 7.83 (d, 1 H, *J* = 16.4 Hz), 7.22 (d, 1 H, *J* = 16.4 Hz), 7.08 (d, 2 H, *J* = 2.2 Hz), 6.68 (t, 1 H, *J* = 2.2 Hz), 3.81 (s, 6 H), 1.74 (s, 6 H, -CH_3); ^{13}C NMR (DMSO-d6, 125 MHz, δ/ppm) 177.7, 175.6, 161.4 (2 C), 147.8, 136.8, 116.6 (2 C), 113.2, 112.4, 111.3, 107.7, 105.0, 100.3, 100.1, 56.2 (2 C), 55.2, 25.6 (2 C); IR (ν/cm^{-1}) 3074, 2981, 2897, 2208, 1584, 1541, 1453, 1340, 1321, 1155, 971; Anal. calcd for $C_{20}H_{17}N_3O_3$: C 69.15, H 4.93, N 12.10; found: C 69.19, H 4.93, N 12.20; MS (ES$^-$, m/z): 346.1 (100 %), 347.1 (21.8 %) for [M-H]$^-$; m.p. > 260°C.

(*E*)-2-(3-cyano-5,5-dimethyl-4-(2,3,4-trimethoxystyryl)furan-2(5*H*)-ylidene)malono-nitrile (1j). From 2,3,4-trimethoxybenzaldehyde **3j** (196 mg) following the general procedure. Red solid (241 mg, yield=64 %). ^{1}H NMR (DMSO-d6, 500 MHz, δ/ppm) 8.22 (d, 1 H, *J* = 16.4 Hz), 7.83 (d, 1 H, *J* = 8.4 Hz), 7.26 (d, 1 H, *J* = 16.4 Hz), 7.02 (d, 1 H, *J* = 8.4 Hz), 3.93 (s, 3 H), 3.90 (s, 3 H), 3.79 (s, 3 H), 1.75 (s, 6 H, -CH_3); ^{13}C NMR (DMSO-d6, 125 MHz, δ/ppm) 177.4, 176.0, 157.6, 153.7, 142.5, 141.7, 125.1, 120.8, 113.7, 112.8, 112.0, 111.5, 108.9, 99.1, 96.3, 61.6, 60.5, 56.3, 53.5, 24.8 (2 C); IR (ν/cm^{-1}) 2944, 2923, 2830, 2228, 1566, 1535, 1496, 1286, 1091, 978, 820; Anal. calcd for $C_{21}H_{19}N_3O_4$: C 66.83, H 5.07, N 11.13; found: C 66.67, H 5.12, N 10.96. MS (ES$^-$, m/z): 378.1 (100 %), 379.1 (25.2 %) for [M+H]$^+$, 400.1 (19.8 %), 401.1 (4.9 %) for [M+Na]$^+$; m.p. > 260°C.

(*E*)-2-(3-cyano-5,5-dimethyl-4-(3,4,5-trimethoxystyryl)furan-2(5*H*)-ylidene)malononitrile (1k). From 3,4,5-trimethoxybenzaldehyde **3k** (196 mg) following the general procedure. Red solid (154 mg, yield=41 %). ^{1}H NMR (DMSO-d6, 500 MHz, δ/ppm) 7.85 (d, 1 H, *J* = 16.4 Hz), 7.27 (s, 2 H), 7.18 (d, 1 H, *J* = 16.4 Hz), 3.87 (s, 6 H), 3.75 (s, 3 H), 1.81 (s, 6 H, -CH_3); ^{13}C NMR (DMSO-d6, 125 MHz, δ/ppm) 177.8, 175.8, 153.8 (2 C), 148.4, 142.0, 130.4, 115.2, 113.3, 112.5, 111.4, 107.9 (2 C), 99.9, 99.2, 60.9, 56.8 (2 C), 54.7, 25.8 (2 C); IR (ν/cm^{-1}) 2992, 2938, 2834, 2227, 1575, 1537, 1498, 1320, 1302, 1125; Anal. calcd for $C_{21}H_{19}N_3O_4$: C 66.83, H 5.07, N 11.13; found: C 66.45, H 5.19, N 11.02; MS (ES$^-$, m/z): 378.1 (100 %), 379.1 (25.1 %) for [M+H]$^+$, 400. 1 (19.8 %), 401.1 (4.9 %) for [M+Na]$^+$; m.p. > 260°C.

(*E*-2-(3-cyano-5,5-dimethyl-4-(2,4,5-trimethoxystyryl)furan-2(5*H*)-ylidene) malononitrile (1l). From 2,4,5-trimethoxybenzaldehyde **3l** (196 mg) following the general procedure. Black solid (188 mg, yield=50 %). ^{1}H NMR (DMSO-d6, 500 MHz, δ/ppm) 8.28 (d, 1 H, *J* = 16.4 Hz), 7.48 (s, 1 H), 7.16 (d, 1 H, *J* = 16.4 Hz), 6.78 (s, 1 H), 3.87 (s, 6 H), 3.93 (s, 3 H), 3.92 (s, 3 H), 3.80 (s, 3 H), 1.74 (s, 6 H, -CH_3); ^{13}C NMR (DMSO-d6, 125 MHz, δ/ppm) 178.2, 177.0, 157.1, 156.0, 144.1, 143.8, 115.1, 113.7, 112.9, 112.8, 112.4, 112.3, 99.3, 97.9, 95.1, 57.3, 56.9, 56.8, 53.2, 25.8 (2 C); IR (ν/cm^{-1}) 2992, 2970, 2897, 2225, 1566, 1503, 1309, 1250, 1206, 1107, 1010; Anal. calcd for $C_{21}H_{19}N_3O_4$: C 66.83, H 5.07, N 11.13; found: C 67.01, H 5.03, N 10.89; MS (ES$^-$, m/z): 378.1 (100 %), 379.1 (24.8 %) for [M+H]$^+$, 400. 1 (20.2 %), 401.1 (4.9 %) for [M+Na]$^+$; m.p. > 260°C.

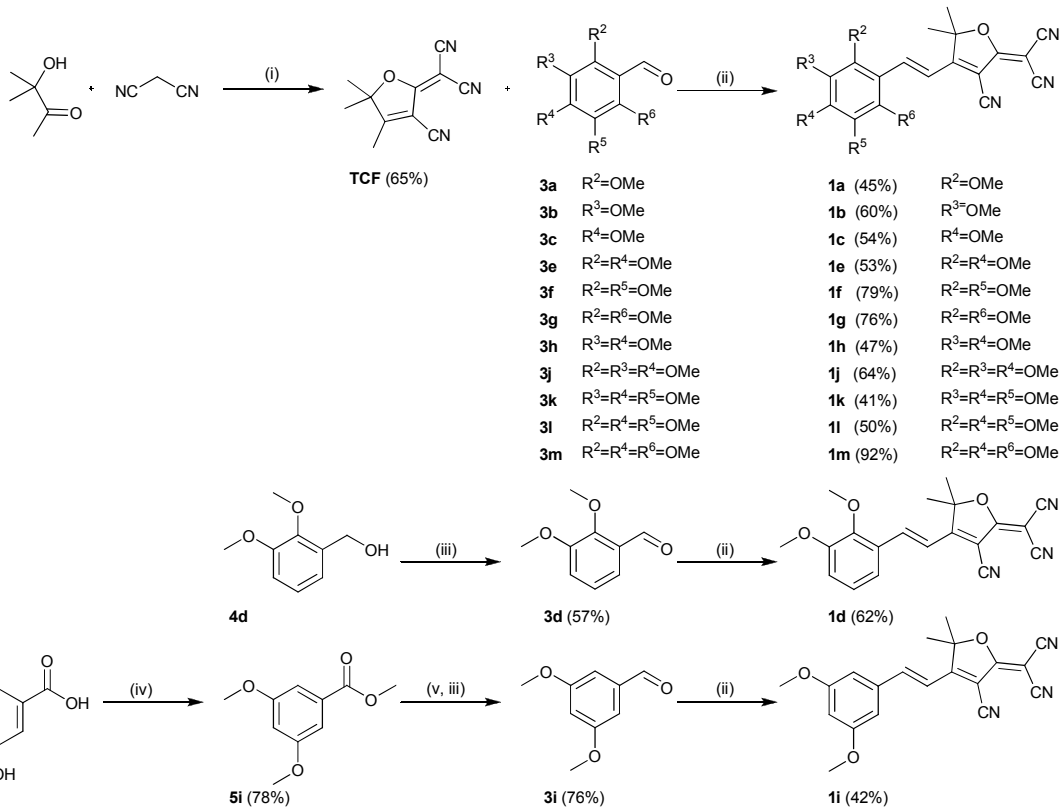

Scheme 1 Synthesis of the solid state fluorophores **1a**-**1m**. Reaction conditions (i) Li (cat.), dry ethanol, reflux, overnight; (ii) piperidine (cat.), dry ethanol, 100°C, 30 min., microwaves; (iii) PCC, CH_2Cl_2, r.t., 24 h; (iv) Me_2SO_4, K_2CO_3, acetone, reflux; 4 h; (v) $LiAlH_4$, Et_2O, 0°C, 1 h.

(*E*)-2-(3-cyano-5,5-dimethyl-4-(2,4,6-trimethoxystyryl)furan-2(5*H*)-ylidene) malononitrile (1m). Starting from 2,4,6-trimethoxybenzaldehyde **3m** (196 mg), the general procedure was followed to give **1m** as violet solid (346 mg, yield=92 %). ^{1}H NMR (DMSO-d6, 500 MHz, δ/ppm) 8.19 (d, 1 H, *J* = 16.4 Hz), 7.35 (d, 1 H, *J* = 16.4 Hz), 6.37 (s, 2 H), 3.95 (s, 6 H), 3.93 (s, 3 H), 1.74 (s, 6 H, -CH_3); ^{13}C NMR (DMSO-d6, 125 MHz, δ/ppm) 177.6, 177.3, 166.1, 162.4, 139.7 (2 C).113.6 (2 C), 113.1, 112.2, 105.7, 98.1, 94.6, 91.5 (2 C), 56.5 (2 C), 56.0, 52.3, 25.8 (2 C); IR (ν/cm^{-1}) 2932, 2225, 1614, 1572, 1542, 1509, 1323, 1257, 1208, 1124, 816; Anal. calcd for $C_{21}H_{19}N_3O_4$: C 66.83, H 5.07, N 11.13; found: C 67.03, H 5.02, N 10.98; MS (ES$^-$, m/z): 376.2 (100 %), 477.2 (21 %) for $[M+H]^+$; m.p. > 260°C.

Crystallography

Single crystals suitable for X-ray diffraction were grown by slow diffusion of cyclohexane in concentrated solution in dichloromethane. Suitable crystals were selected and mounted on a Gemini kappa-geometry diffractometer (Agilent Technologies UK Ltd) equipped with an Atlas CCD detector and using Mo radiation (λ=0.71073 Å). Intensities were collected at 100 K or 150°K by means of the CrysalisPro software. Reflection indexing, unit-cell parameters refinement, Lorentz-polarization correction, peak integration and background determination were carried out with the CrysalisPro software.[26] An analytical absorption correction was applied using the modeled faces of the crystal.[27] The structures were solved by direct methods with SIR97 [28] and the least-square refinement on F^2 was achieved with the CRYSTALS software.[29] All non-hydrogen atoms were refined anisotropically. The hydrogen atoms were all located in a difference map, but were then repositioned geometrically. The H atoms were initially refined with soft restraints on the bond lengths and angles to regularize their geometry (C—H in the range 0.93-0.98 Å) and U_{iso}(H) (in the range 1.2-1.5 times U_{eq} of the parent atom), after which the positions were refined with riding constraints. CCDC 1429526 (**1c**), 1429527 (**1d**), 1429528 (**1e**), 1429529 (**1g**), 1429531 (**1i**), 1429530 (**1j**) and 1429532 (**1m**) contains the supplementary crystallographic data for this paper. These data can be obtained free of charge from The Cambridge Crystallographic Data Centre via www.ccdc.cam.ac.uk/data_request/cif.

Spectroscopic measurements and solid-state fluorescence

Absorption spectra were recorded on a JASCO V670 spectrophotometer. Fluorescence spectra (excitation and emission) were measured using a Horiba-Jobin Yvon Fluorolog-3 spectrofluorimeter equipped with a Hamamatsu R928 photomultiplier tube. Spectra were reference corrected for both the excitation source light intensity variation (lamp and grating) and the emission spectral response (detector and grating). All solvents were of spectrophotometric grade. Solid-state measurements were performed using a calibrated integrative sphere collecting all the emission (2π steradians covered with spectralon®), model F-3018 from Horiba Jobin

Yvon. The sphere was calibrated with known standard (Coumarin 153, Rhodamine 6G, DMANS, erythrosine B and tetraphenylporphyrin).[30] Quantum yield were measured as described by de Mello *et al.*[31] and Porrès *et al.*[32]. For each sample, four measurements were made using the same excitation and emission monochromatic bandpass (slits opening) to give four integrated intensities. Quantum yield are therefore given by the following equation:

$$\Phi_F = \frac{E_{in} - E_{empty}}{ND \times (L_{empty} - L_{in})}$$

where E_{in} and E_{empty} are the integrated fluorescence resulting of a direct excitation of the sample and the integrated fluorescence without any sample (the background of the sphere), L_{empty} is the integrated excitation profile with the empty sphere, and L_{in} is the integrated excitation profile with the sample inside the sphere. For the determination of L_{empty} and L_{in}, neutral density filter (*ND=0.5%*) was used to reduce the intensity without changing the excitation profile.

Agregation-induced emission measurements

Stock solutions (1 mM) of the desired compound were prepared in THF. For each water fraction (f_w), 100 µL of this solution were added in a 2 mL volumetric flask, followed by the required volume of THF. Water was then added one-shot to reach 2 mL. The mixture was sonicated for 30 s, and allowed to rest for 2 min before the measurement.

Two-photon absorption

Measurements of solid-state two-photon excitation spectra were performed on 8-mm pellets of microcrystal powders compacted with a manual press. A Ti:sapphire mode-locked femtosecond laser (Tsunami, Spectra Physics Inc., USA) with a pulse duration of 100 fs, a repetition rate of 82 MHz, and a tunable spectral range from 700 nm to 920 nm was used with a constant average power of 110 mW. The two-photon pellet fluorescence was obtained by a direct beam irradiation (1/e² diameter <2 mm), without focalization, to obtain a spatial averaging of microcrystal orientations and sizes. The fluorescence signal was collected from the sample front surface at 90° with respect to the excitation beam direction. The sample surface was slightly off 45° to reflect the excitation beam out of the collection system. The fluorescence signal, after passing through a short-pass filter (700 nm), was focused into an optical fiber (diameter: 400 µm) connected to an Ocean Optics S2000 spectrometer. The detector integration time was fixed to 25 ms. The quadratic dependence of the TPA on the excitation intensity was checked to exclude possible artefacts.

Results and Discussion

Synthesis

All compounds were obtained through a final Knoevenagel condensation between **TCF** (**2**) and the corresponding benzaldehyde (**3a**-**m**) according to Scheme 1. This reaction was performed under micro-wave irradiation in anhydrous ethanol with few drops of piperidine as catalyst. This simple method has been shown to give better yield than traditional heating [33] and enabled the recovery of the precipitated crude product by simple filtration with decent yields from 42 % (for **1a**) to 79 % (**1f**). Flash column chromatography was needed to get rid of a bluish minor by-product standing at the top of the column which quenched the solid-state fluorescence.

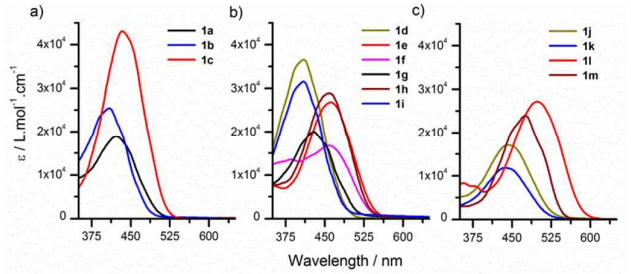

Fig. 1 Absorption spectra in THF of (a) the monomethoxy- **1a**-**1c**, (b) the dimethoxy- **1d**-**1i**, and (c) the trimethoxy-TCF dyes **1j**-**1m**.

Optical properties in dilute solution

The optical properties of all dyes **1a**-**1m** were measured in solution (10 µM) in THF which was chosen because of its medium polarity. Relevant photo-physical data are reported in Table 1. All solutions exhibit strong yellow to orange color except for **1l** which is more violet. Absorption spectra (Fig. 1) present broad bands in the visible with maxima varying from 409 nm (**1i**) to 498 nm for **1l**, characteristic of induced charge transfer (ICT) in push-pull dipolar molecules. Increasing the number of methoxy groups causes a red-shift of the absorption due to a more pronounced ICT: the three monomethoxy compounds **1a**-**c** absorb under 435 nm, whereas all trimethoxy ones (**1j**-**m**) present a maximum of absorption above this value. As expected, positions *meta* are the less favorable for conjugation with the TCF group and the associated compounds (**1b**, **1d**, **1i**) present the most blue shifted absorption. The *para* position induces a more pronounced red-shift in absorption (433 nm for **1c**) than the *ortho* one (420 nm for **1a**). As a reminder, *ortho*, *meta* and *para* always refer to the positions of the methoxy with respect to the electron-accepting group. More surprisingly, dramatic red shifts of the absorption maxima are observed when two methoxy groups are positioned *para* to each other compared to other substitution patterns. For example, the structures of **1d** (2,3-diMeO) and **1f** (2,5-diMeO) are very similar with two methoxy groups in *ortho* and *meta* positions relative to the TCF group, but **1f** presents a 50 nm red-shift of the maximum absorption wavelength compared to **1d** (2,3-diMeO). This is even more flagrant when comparing in the cases of **1j** (2,3,4-triMeO) and **1l** (2,4,5-triMeO), where the three methoxy groups occupy one *ortho,* one *meta* and the *para* position relative to the TCF group. Moving one methoxy substituent from one *meta* position (**1j**) to the second *meta* position but placed *para* to another methoxy (in **1l**) induces a 60 nm red shift in the absorption maximum peak. The molar extinction coefficients of the charge transfer band are ranging from 15000 to 30000 $L.mol^{-1}.cm^{-1}$ with the exception of **1k** which

Table 1 Optical properties of compounds 1a-1m in solution, in self-aggregate (THF/water mixture) and in solid (powder)

	Solution (THF and ethylene glycol)				Self-aggregate (THF/water mixture)			Solid (powder)	
	λ_{abs} (nm) [a]	ε ($M^{-1}.cm^{-1}$) [a]	λ_{em} (nm) [b]	Φ_f (%) [b,c]	λ_{em} (nm) [d]	Φ_{SA} (%) [d, e]	Enhan. [f]	λ_{em} (nm) [g]	Φ (%) [e]
1a	421	18 800	567	< 1	576	25	200	620	28
1b	410	21 900	550	< 1	562, 593	< 1	245	612	4
1c	433	43 000	560	2	622	10	61	615 (s), 666	15
1d	411	31 000	578	< 1	598	3	31	550 (s), 580, 625 (s)	13
1e	462	19 500	573	3	610	9	58	704	7
1f	458	14 900	675	2	649	-	< 0	658	2
1g	429	19 600	552	< 1	578	6	240	596 (s), 624	21
1h	459	28 900	594	6	618	13	30	634	20
1i	409	27 300	559	< 1	622	< 1	30	646	<1
1j	442	18 200	572	2	620	7	35	645	26
1k	438	11 600	617	6	610	-	< 0	644	1
1l	498	23 600	635	4	-	-	< 0	732	5
1m	476	22 900	570	2	620	7	147	644 (s), 679	22

[a] in THF; [b] in ethylene glycol; [c] using Erythrosin B in methanol (Φ=9%) as reference. [d] measured in THF/water mixture for f_w giving the maximal intensity; [e] absolute quantum yield measured using a calibrated integrative sphere; [f] ratio between the intensity of emission in THF solution and the maximal intensity of emission in THF/water (f_w giving the maximal intensity); [g] (s) stands for shoulder.

presents a weaker absorption (11600 $L.mol^{-1}.cm^{-1}$) and **1c** which absorbs much more (43000 $L.mol^{-1}.cm^{-1}$).

Upon excitation in the CT band, dyes **1a**-**1m** barely show any fluorescence in THF. However, an emission appears in more viscous solvent like ethylene glycol and glycerol as shown in Fig. 2a, that is characterized by a large Stokes' shift (from 3465 cm^{-1} for **1m** to 7030 cm^{-1} for **1d**) typical of this type of push-pull fluorophores. The maxima of emission in ethylene glycol range from green to orange and red, from 550 nm for **1b**, **1g** or **1i** to 675 nm for **1f** (Fig. SI-2 and SI-3). The quantum yields of emission (Φ_f) were measured in ethylene glycol. Φ_f values remained low only reaching 6% at 594 nm and 617 nm for the most fluorescent compounds **1h** and **1k**. The fluorescence considerably increases when further increasing the viscosity with solvent system like 90/10 glycerol/methanol or when freezing the medium (90/10 glycerol/methanol at -10°C) as illustrated for compound **1h** in Fig. 2b (see also Fig. SI-4). Note that, even though most emission quantum yields remain low, all the compounds show an increase in emission

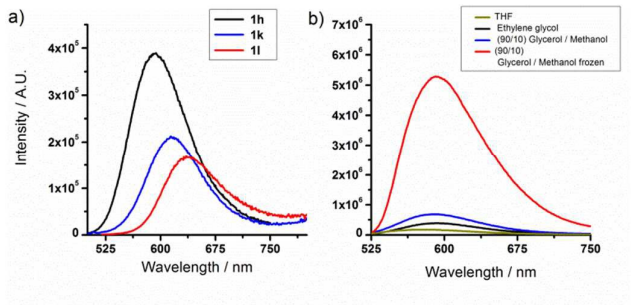

Fig. 2 (a) Emission spectra of **1h**, **1k** and **1l** in ethylene glycol; (b) Emission spectra of **1h** in different solvents THF, ethylene glycol, 90/10 glycerol/methanol and frozen 90/10 glycerol/methanol (-10°C).

when the viscosity increases. These observations are in agreement with previous report by Font-Sanchis *et al*. on 4- and 2,4,5-alkoxy-TCF derivatives with structure very similar to **1c** and **1l**.[24b] With the help of theoretical calculations combined to laser flash photolysis experiment these authors attributed the large Stoke shift to relaxation from the Franck-Condon state to an emissive TICT state, via rotation around the $C=C(CN)_2$ bond, and the low quantum yield in emission by the formation of a non-emissive excited dimer between an excited monomer and a monomer at the ground state. *Cis-trans* isomerization was also proposed as competitive mechanism to explain the low fluorescence. The two mechanisms are not exclusive and may be postulated here as well. Increasing the viscosity prevents the dimer formation by slowing down the diffusion, hence restoring the fluorescence. This does not exclude an additional fluorescence increase by restrictions of the intramolecular movements, slowed down in viscous media, and indicates that the emission is highly sensitive to the local environment and the rigidity in particular. As restriction of intramolecular motions is now clearly identified as the major process explaining the aggregation induced emission phenomenon,[15] these observations highlight the potential of dyes **1a**-**1m** for AIE by inhibition of the free intramolecular rotations.

Aggregation induced emission

To highlight eventual solid state fluorescence properties, we proceed to nano-precipitation experiments and follow the evolution of the absorption and of the fluorescence of **1a**-**1m** after adding a concentrated solution of compound to different THF/water mixture having various water fractions (f_w) and so that the final concentration was kept constant at 50 µM. This water-borne reprecipitation method is one of the best

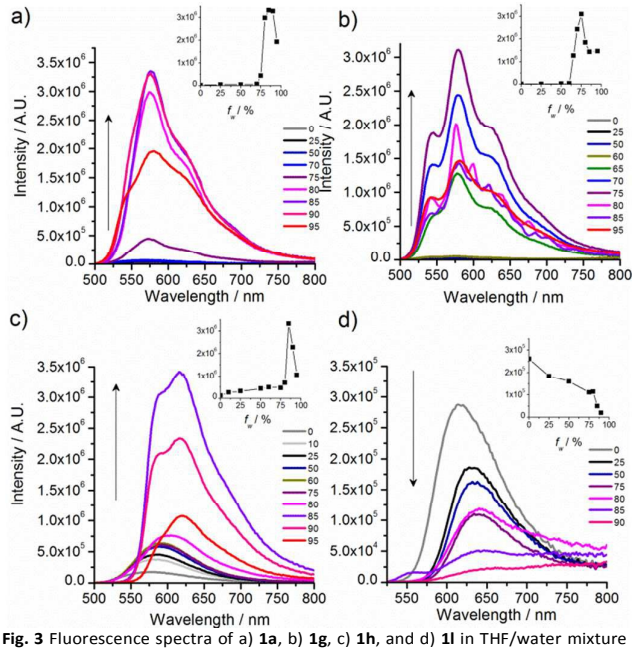

Fig. 3 Fluorescence spectra of a) **1a**, b) **1g**, c) **1h**, and d) **1l** in THF/water mixture with different water fraction (f_w). Insets: change of peak intensity with f_w.

techniques for fabricating organic nanocrystals.[34] Water is a nonsolvent that lowers the solubility but also stabilized the colloidal dispersion formed by promoting surface charge. For low water fraction, the solvent mixture still dissolves the compound, whereas at higher water fraction precipitation occurs. Fig. 3 shows the fluorescence spectra at different ratios f_w for dyes **1a**, **1g**, **1h**, **1l** as well as the variations of the intensity as a function of f_w. Absorption data and fluorescence data for other compounds are given in SI (Fig SI-5 to SI-17). Very different results were obtained depending on the compounds, highlighting how small variations in the molecular structure can dramatically influence the emission in the aggregated state. For most compounds indeed, precipitation was accompanied by a significant increase in the fluorescence, together with a gradual red shift of the emission and a severe broadening of the absorption spectra. This is typical of the AIE phenomenon. Only for **1d** a small blue shift of 20 nm was observed. In most cases, after reaching a maximum or a plateau, the fluorescence significantly decreases when further increasing the water ratio f_w. This alteration in the fluorescence can be explained by the formation stable nano-aggregates at high water fractions rather than bulk precipitation for low water fraction 50-70%.[35] The emission quantum yields of the different suspensions were measured using a calibrated integrating sphere for f_w giving the maximum intensity (Table 1). They vary from very low (< 1 %) to quite high reaching 25 % for the most emissive compound **1a**. Interestingly, intense fluorescence above 600 nm can be reached with **1m** (7 % at 650 nm). Finally, even for the least fluorescent compounds (**1b** and **1i**), considerable enhancement was observed in the fluorescence (up to 240 for **1g**) between the homogeneous solution in THF and the aggregate state.

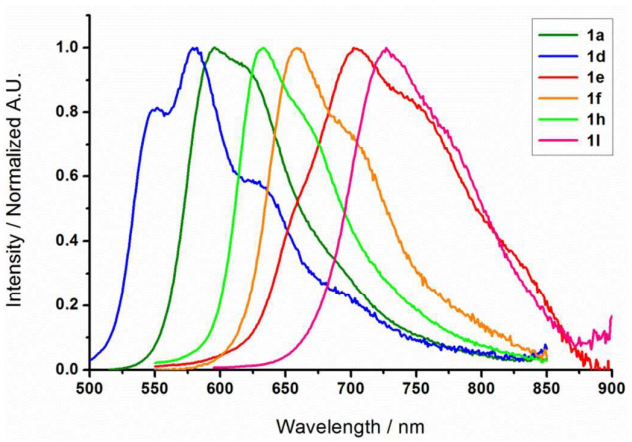

Fig. 4 Solid emission spectra of **1a**, **1d**, **1e**, **1f**, **1h** and **1l** showing the span in the emission range.

In contrast, for three compounds, **1f**, **1k** and **1l**, a decrease in fluorescence together with a blue shift in emission was observed when water was added. The fluorescence was even completely quenched at high water fraction precipitation for compounds **1f** and **1k**. Oddly enough, these compounds had similar properties to the other derivatives in viscous solvent, showing an increase in fluorescence when the viscosity increased and fluorescence quantum yields in ethylene glycol between 2 and 6 %.

These observations allow concluding that the AIE phenomenon depends strongly on the substitution. Furthermore, in the aggregated state torsional motions are unambiguously minimized, as proved by the fluorescence enhancement observed for most compounds, but obviously further factors influence the fluorescence, such as molecular distances and arrangements. Although a strong fluorescence enhancement was observed for almost all the molecules with respect to the dilute solution in THF, quantum yields remain modest and the emission maxima are below 700 nm.

Solid-state fluorescence

Spectroscopic measurements were performed directly on the powder. First of all, it is worth noting that, with the exception of compound **1i**, all powders exhibit fluorescence under UV irradiation (365 nm), even **1f**, **1k** and **1l**, the three derivatives not showing AIE. Solid-state spectroscopic data are summarized in Table 1. Excitation and emission spectra are shown in Fig. 4 and in SI (Fig. SI-17 to SI-29). The influence of the MeO substituents (number and positions) on the solid state emission properties is especially evidenced by the variation of the emission maxima. Emission spectra are broad and the maxima span all the orange-red part of the visible, ranging from 580 nm in the case of *2,3*-diMeO-TCF **1d** to over 730 nm for *2,4,5*-triMeO-TCF **1l**, *i.e.* a difference of about 150 nm. For comparison, in solution the difference between the two extreme emission maximum wavelengths was 125 nm (550 nm for **1b**, 675 nm for **1f**). Actually the emission maxima are considerably red-shifted in solid relative to the solution and the suspension, with a maximum shift of more than 100 nm to the red for **1e**. This indicates that the arrangements

of the molecules in the solid state are different in powder and self-aggregate suspension. As for solution, the substitution pattern inducing the most red-shifted emission is 2,4,5 (compound **1l**, having a maximum of emission at 732 nm), where two MeO groups are conjugated (*ortho* and *para*) with the electron-withdrawing TCF group and one MeO is not in conjugation with the TCF group (*meta* postion) but placed in *para* from another MeO group. Interestingly the other *ortho*, *meta*, *para* derivatives (compound **1j**, 2,3,4-trimethoxy-TCF) in which the *meta* MeO group is situated in *ortho* to the other two MeO groups has a maximum of emission at 645 nm only. In turn, the excitation spectra (Fig. SI-17 to SI-29) of the emissive compounds are broad and some (**1d**, **1f**, **1g** and **1h** and to a lesser extent **1a**, **1j** and **1m**) present a strongly bathochromically shifted band with a smaller Stokes shift relative to the solution or the suspension suggesting the formation of *J*-like assemblies.

For a quantitative comparison, the fluorescence quantum yields (Φ_F) of the molecules were measured. As expected, the Φ_F values are much higher in powder than in solution but also 3.5 to 5 times higher than in suspension. If there is a rather high uncertainty on the quantum yield measurement, certain coherence in the values can nevertheless be pointed out. compounds **1a**, **1c**, **1e** and **1h** display similar emission quantum yield in powder and self-aggregate and compounds which do not exhibit AIE (*i.e.* **1f**, **1k** and **1l**) are the less fluorescent in powder with quantum yields between 1 and 5 %. Intense far red fluorescence is usually associated with longer conjugated molecules, such as long A–π–D–π–A framework (33 % quantum yield at 702 nm),[18h] organo-boron derivatives having either a seven-ring fused π-conjugated skeleton (41 % at 670 nm)[36] or complexed to 2'-hydroxychalcones (0.5 % at 855 nm and almost 20 % at 722 nm)[18k] or also lipidic-bodipy dyes self-assembling in nanoparticles (6 % at 743nm)[37] to cite a few. That is why quantum yield values over 20 % in the red, 21 % at 596 nm (**1a**, **1g**), 20 % at 634 nm (**1h**), 26 % at 645 nm (**1j**) and 22 % at 679 nm (**1m**), are remarkable for such small and simple molecules. Even more noteworthy are the values for **1e** and **1l**, up to 5-7 % for emission beyond 700 nm (respectively 704 and 732 nm).

Crystal Structure

Analysis of the crystal structures and crystal packing have been shown to be important to understand the optoelectronic properties and correlate the fluorescence properties in the solid state to specific arrangements in the crystal.[18a, 18g, 18m, 20a, 38] Crystals suitable for X-ray diffraction were obtained for six over thirteen compounds: one monomethoxy (**1c**), four dimethoxy (**1d**, **1e**, **1g**, and **1i**), and one trimethoxy compound (**1j**). **1c**, **1d**, **1g**, and **1j** are fluorescent whereas **1e** is weakly fluorescent and **1i** is not fluorescent. All crystals were grown by slow diffusion of diisopropylether in concentrated solution in chloroform. Crystallographic data, refinement parameters and basic structural parameters are given in Table 2 as well as in SI. The atom numbering scheme common to all structures with the angle and distances definition is given in Supporting Materials (Fig. SI-1) whereas selected distances and dihedral angle are compiled in Table SI-1. Monomethoxy **1d** crystallized in the monoclinic $P2_1/m$ space group with an elemental cell containing two molecules. Dimethoxy **1d** and **1g** crystallized in the monoclinic $P2_1/c$ space group with four molecules in the elemental cell, whereas **1e** and **1f** crystallized in the orthorhombic *Pbca* and *Pnma* space groups with respectively eight and four molecules in the elemental cell.

Finally, trimethoxy **1j** crystallized in the monoclinic $P2_1/m$ space group with an elemental cell containing four molecules.

Table 2 Crystal data and structure refinement parameters

	1c	**1d**	**1e**	**1g**	**1i**	**1j**	**1m**
Formula	$C_{19}H_{15}N_3O_2$	$C_{20}H_{17}N_3O_3$	$C_{20}H_{17}N_3O_3$	$C_{20}H_{17}N_3O_3$	$C_{20}H_{17}N_3O_3$	$C_{21}H_{19}N_3O_4$	$C_{21}H_{19}N_3O_4$
Cryst. Syst.	Monoclinic	Monoclinic	Orthorhombic	Monoclinic	Orthorhombic	Monoclinic	Monoclinic
Space group	$P2_1/m$ (N° 11)	$P2_1/c$ (N° 14)	*Pbca* (N°61)	$P2_1/c$ (N° 14)	*Pnma* (N° 62)	$P2_1/n$ (14)	$P2_1/c$ (N° 14)
a (Å)	10.0110(9)	8.0071(5)	13.854(2)	10.397(2)	17.1210(10)	15.229(2)	16.2981(11)
b (Å)	6.9999(6)	15.2752(8)	15.110(2)	9.8280(10)	6.9428(5)	7.5088(7)	16.4911(9)
c (Å)	11.5760(10)	14.9890(10)	16.697(3)	17.179(2)	15.4460(10)	16.6390(10)	7.1281(5)
α (°)	90	90	90	90	90	90	90
β (°)	101.360(10)	102.870(6)	90	94.990(10)	90	92.397(7)	100.738(6)
γ (°)	90	90	90	90	90	90	90
V (Å3)	795.307	1785.14	3495.25	1748.7(4)	1836.03	1901.03	1882.3
Z	2	4	8	4	4	4	4
T	100	150	150	150	150	150	100
D_{cald} (g.cm^{-3})	1.325	1.292	1.320	1.319	1.257	1.319	1.332
μ (mm^{-1})	0.72	0.73	0.74	0.74	0.71	0.77	0.77
θ *range* (°)	3.9-66.3	4.1-67.0	4.9-67.0	4.2-67.8	5.1-67.0	2.8-66.9	3.8-67.1
total no. data	8943	19637	16513	13075	11309	17984	24328
no. unique data	1533	3163	3110	3103	1772	3353	3349
no. params refined	150	236	236	236	162	253	260
R_1	0.045	0.046	0.062	0.066	0.039	0.069	0.073
wR_2	0.106	0.086	0.111	0.204	0.113	0.141	0.204
GoF	0.94	1.01	1.03	1.00	1.01	1.07	1.07

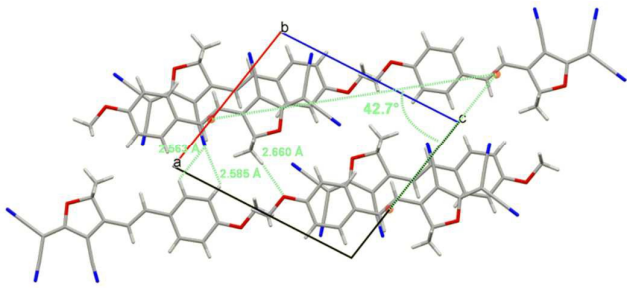

Fig. 5 Packing diagram of **1c**, viewed down the crystallographic *b* axis showing the brickwork arrangement.

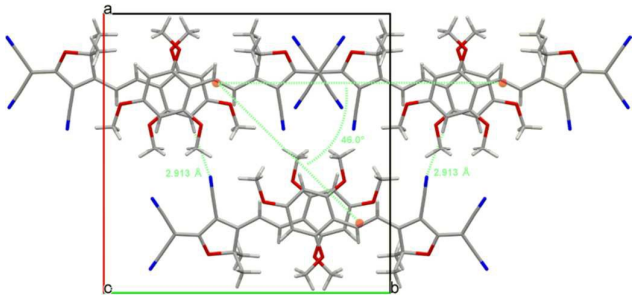

Fig. 6 Partial view of the packing of **1m** viewed down the crystallographic *c* axis showing the brickwork arrangement.

At a molecular level no noticeable differences come into view as the structures are very similar for all compounds. Only the all *trans* rotamer is present and a s-*trans* conformation of the electron accepting group relative to the central b_1 double bond in accordance with similar D-π-A molecules.[20a, 39] The conjugated system is almost planar with only slight variation from planarity to the donor end of the molecule with a maximum dihedral angle α between the plane of the phenyl ring and the plane formed by the rest of the conjugated system of 12.6° for **1g**. The π-conjugated systems also present good alternations of C-C single and double bonds indicating a full delocalization between the donor and the acceptor end.

Representative aggregates can be observed in the crystal packing of the fluorescent solids **1c**, **1e**, **1d**, **1g**, **1j** and **1m**, in which all the molecules are slipped away from one another prevented close packing. Shifted chains of single lines dipoles create brickwork pattern (**1c**, **1e**, **1m**) or broken lines leading to herringbone motif (**1d**, **1j**, and **1g**).[40] Unfortunately, there is no clear influence of the number and the relative position of the methoxy groups on the molecular packing. The oxygen atom of the methoxy groups is sometimes involved in H-interaction with aromatic or vinylic hydrogen of a neighboring molecule (see **1c** and **1i**) linking two parallel chains of in-line molecules, but this is only one among many interactions that does not explain the full packing and the difference observed. Crystal packing of **1c** (Fig. 5), **1m** (Fig. 6) are best described in terms of in-line dipoles forming infinite chains parallel to each other. Two neighboring chains stand less than 3 Å apart but are longitudinally displaced with a slip angle of 42.7° for **1c** and 46.0° for **1m** with respect to each other creating the brickwork arrangement in which two consecutive layers lying *ca* 3.5 Å apart are packed antiparallel. Moreover, in the packing of **1c**, multiple H-interactions exist between the oxygen atom of the

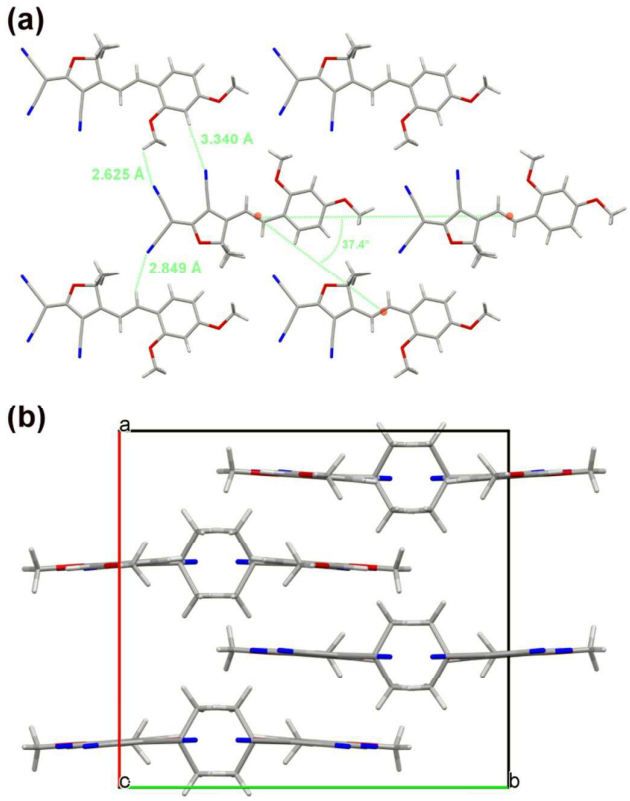

Fig.7 Partial view of the packing of **1e** showing the brickwork arrangement (a) and packing diagram of **1e** viewed down the crystallographic *c* axis (b).

methoxy group and hydrogen atoms of the two TCF methyl groups of a neighboring molecule of the nearest chain (*d*=2.660 Å), and between the central C≡N group and two aromatic hydrogen atoms (*d*=2.563 Å and 2.585 Å). In the case of **1m**, only one H-interaction (*d*=2.913 Å) between the central C≡N group of a molecule and the aromatic hydrogen of its closer neighbor in another chain could be seen. The packing of **1e** (Fig. 7) is composed of strata made of two identical planes of molecules aligned in the (*O, c*) direction but longitudinally displaced (slip angle 37.4°) with respect to each other. Multiple H interactions connect the lines. In every plane and between two consecutive planes the lines are shifted preventing close packing and creating the brickwork arrangement.

The packing of **1g** is rather complicated (Fig. 8) mixing brickwork and herringbone motifs. Layers piled up parallel to the (*0, 0, 1*) crystallographic plane are made of anti-parallel chains of in-line dipoles creating a kind of brickwork pattern. However, unlike **1c** or **1e**, the molecular planes are perpendicular to the layer plane. Along the (*O, c*) direction, two consecutive layers are twisted by 83.07° creating the overall herringbone pattern. The herringbone type packing of **1d** is best viewed down crystallographic *c* axis. This view (Fig. 9) reveals accentuated vertices of 28° created by multiple H-interactions between two C≡N groups of one molecule and aromatic and the methyl ($-CH_3$) hydrogen atoms of two neighboring molecules.

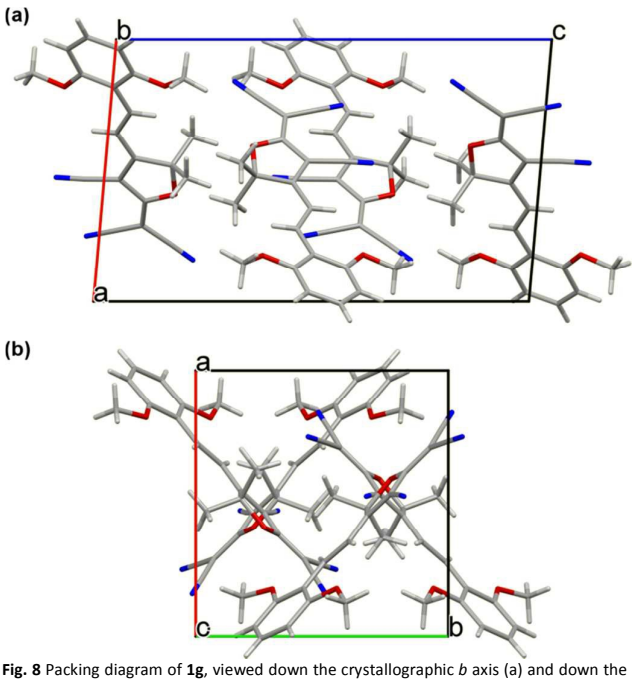

Fig. 8 Packing diagram of **1g**, viewed down the crystallographic *b* axis (a) and down the crystallographic *c* axis (b) showing the mix of brickwork and herringbone arrangement.

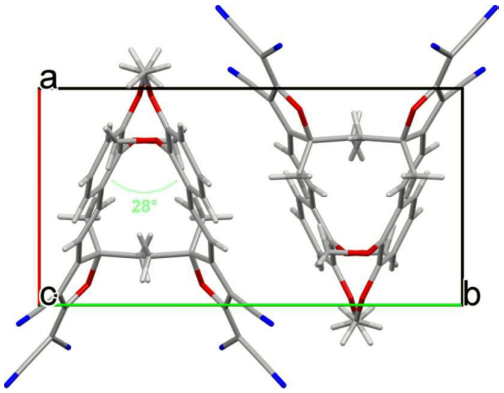

Fig. 9 Packing diagram of **1d**, viewed down the crystallographic *c* axis showing the typical herringbone arrangement.

The packing of **1j** (Fig. 10) can also be described as a herringbone pattern whose repeating unit is composed of two anti-parallel in-plane molecules connected by H-interactions (*d*=2.712 Å and *d*=2.561 Å) between the two C≡N groups and two aromatic hydrogen atoms. View down crystallographic *c* axis reveals the herringbone pattern parallel to the (*0, 0, 1*) crystallographic plane created by repeated units turned by 64° from each other. The interconnection between two broken lines occur by packing (3.566 Å) of two head-to-tail molecules slipped away laterally. Along the (*O, c*) direction, dipole arrange in-line slightly tilted from an average plane.

In contrast, in the case of the non-fluorescent compound **1i** (Fig. 11), close stacking (3.471 Å) of head-to-tail dipole results in typical *H*-type aggregate. Face-to-face superimposition of π-conjugated systems create piles growing along the (*O, b*) direction. Every pile is connected to four neighboring ones turned by 90° by H-interactions, in particular between the

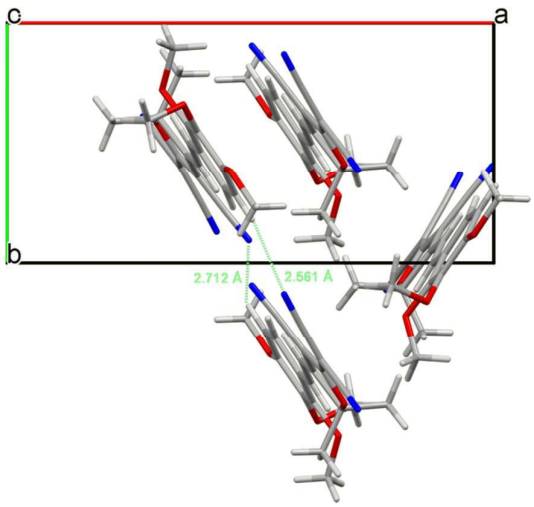

Fig. 10 Packing diagram of **1j**, viewed down the crystallographic *c* axis showing the herringbone arrangement

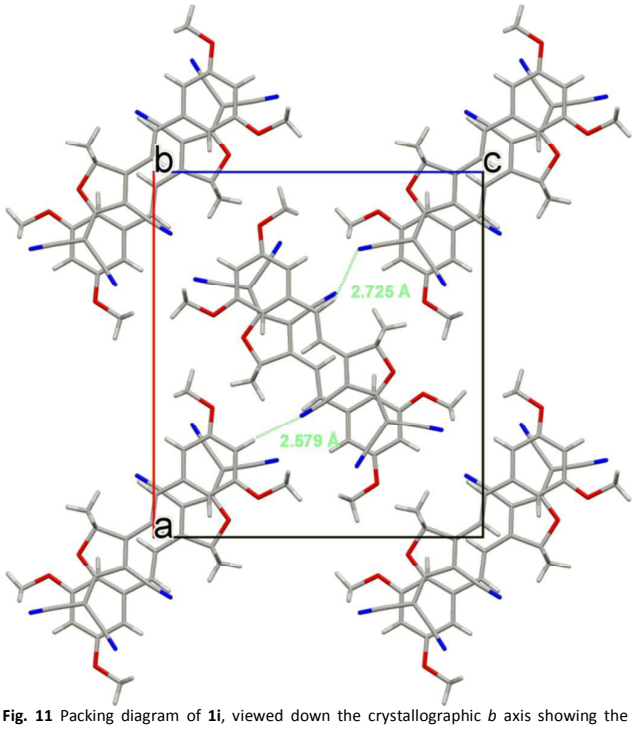

Fig. 11 Packing diagram of **1i**, viewed down the crystallographic *b* axis showing the tightly close packing of the molecules.

central C≡N and the aromatic para-hydrogen atom situated between the two methoxy groups (*d*=2.579 Å).

Two-photon excited fluorescence on the solid-state.

Owing to the strong push-pull dipolar character of compounds **1a**-**1m**, interesting nonlinear optical properties, and in particular two-photon absorption properties, can be expected. Measurements of biphotonic excitation spectra were carried out using a Ti:sapphire laser (tunable along the 720-900 nm range). Emission signals were indeed observed for all fluorescent solids under excitation at 800 nm, which quadratic variations of the intensity as a function of the laser power

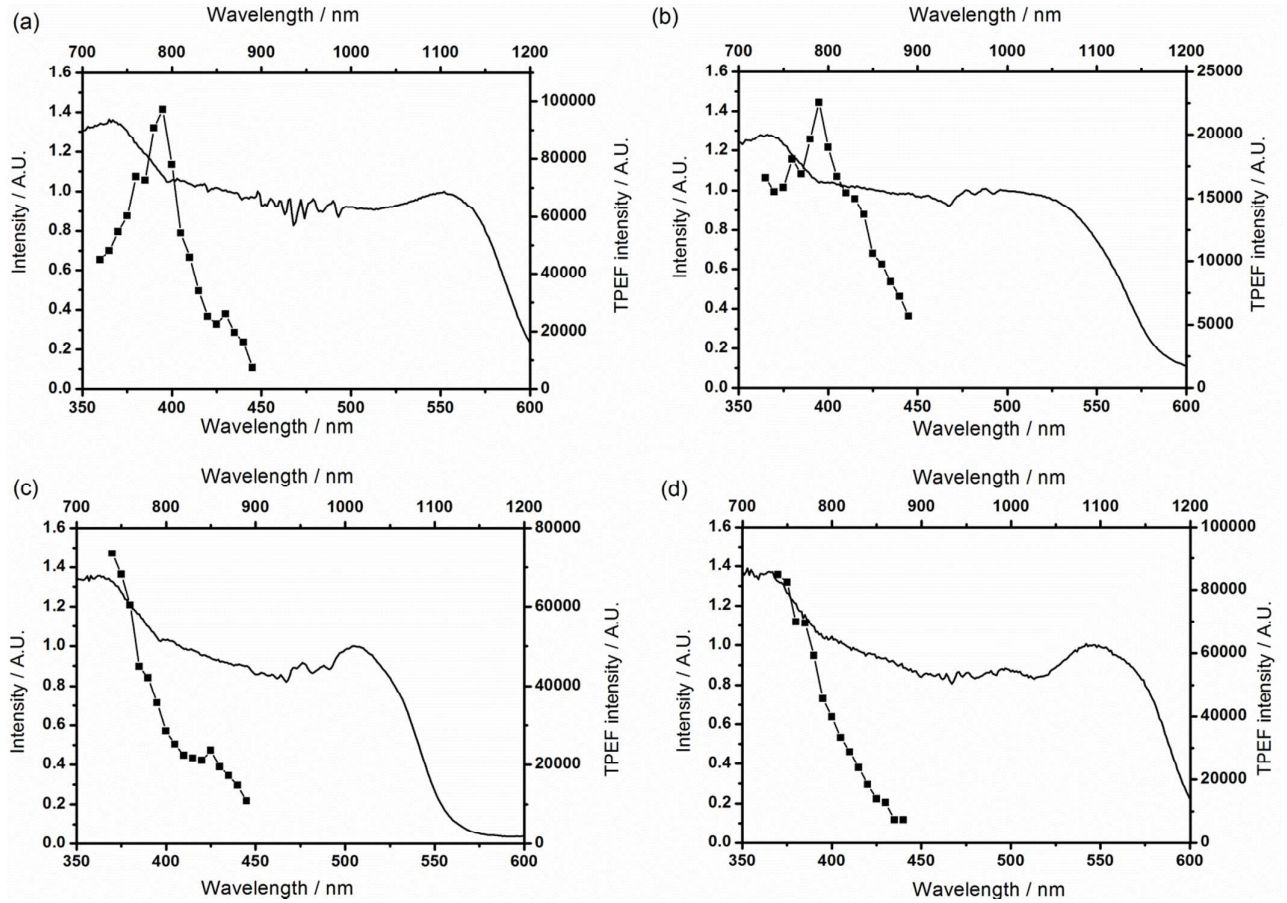

Fig. 12 One photon (line) and two-photon excitation spectra corrected from the quantum yield (scatter + line) of compounds: (a) **1a**, (b) **1b**, (c) **1d**, and (d) **1g** in solid (powder).

illustrate the biphotonic origin (Fig. SI-30). However, recording two-photon excitation spectra in the low wavelength range of the Ti:sapphire laser was not possible for all compounds. For some of them (**1c**, **1e**, **1f**, **1h**-**1l**), which present a linear excitation cut-off beyond 650 nm (see Fig. 5) an overlap between one and two-photon excitation was expected. Consequently, the measurements were only carried out for **1a**, **1b**, **1d** and **1g** that have the less red-shifted excitation spectrum and a one-photon excitation cut-off below 650 nm. Fig. 13 shows the two-photon excitation spectra in the 720-900 nm range, corrected from the emission quantum yield. The four compounds display broad band biphotonic spectra on solid with a maximum absorption $\lambda^{(2)}_{max}$ around 790 nm for **1a** and **1b** while for **1d** and **1g** the maxima are below 700 nm. As expected compound **1b** in which the MeO donor group is positioned *meta* relative to the TCF group and therefore the less conjugated, is by far the less efficient.

Conclusions

In summary, we have designed and synthesized a novel family of far-red solid-state emitters based on the strong electron-withdrawing group TCF. The easy synthesis allowed the engineering of a lot of different methoxy substituted styryl-TCF fluorophore varying by the number and the position of the methoxy groups. The compounds barely show any emission in solution, but see their fluorescence increased when the viscosity of the solvent increases. Typical AIE was demonstrated with a red-shifted and enhanced emission upon addition of water and fluorescence quantum yield (Φ_f) up to 25 % measured at 575 nm (for **1a**) and 13 % at 616 nm for **1h**. More interestingly, we demonstrated that small structural variations have a drastic impact on the solid-state emission and modulate the emission wavelength by 150 nm from 580 nm for **1d** to 730 nm for **1l** also influencing the emission efficiency. Compounds **1a**, **1g**, **1h** and **1i** are of particular interest for their high quantum yield (Φ_f > 20 %) with emission over 620 nm. Near infra-red (730 nm) was also reached with **1l** (Φ_f = 5 %) which is quite unusual for such small molecules. Preliminary results on two-photon absorption in solid reveal the great potential of these rather simple fluorophores combining high solid-state emission and two-photon absorption in the range 800-900 nm for the development of fluorescent nanoparticles for two-photon excited fluorescence bio-imaging.[7b, 8a, 41]

Acknowledgements

This work was performed with the support of the French National Research Agency (Ultrabright-Tracers ANR-11-BS08-0017).

Notes and references

1 (a) C. D. Müller, A. Falcou, N. Reckefuss, M. Rojahn, V. Wiederhirn, P. Rudati, H. Frohne, O. Nuyken, H. Becker and K. Meerholz, *Nature*, 2003, 421, 829; (b) C.-T. Chen, *Chem. Mater.*, 2004, 16, 4389; (c) J. G. C. Veinot and T. J. Marks, *Accounts Chem. Res.*, 2005, 38, 632; (d) P.-T. Chou and Y. Chi, *Chem. Eur. J.*, 2007, 13; (e) Y. Liu, X. Tao, F. Wang, X. Dang, D. Zou, Y. Ren and M. Jiang, *J. Phys. Chem. C*, 2008, 112, 3975.

2 (a) U. Scherf, S. Riechel, U. Lemmer and R. F. Mahrt, *Curr. Opin. Solid St. M.*, 2001, 5, 143; (b) I. D. W. Samuel and G. A. Turnbull, *Chem. Rev.*, 2007, 107, 1272; (c) D. Zhang, V. Martín, I. García-Moreno, A. Costela, M. E. Pérez-Ojeda and Y. Xiao, *Phys. Chem. Chem. Phys.*, 2011, 13, 13026.

3 W. Qin, J. W. Y. Lam, Z. Yang, S. Chen, G. Liang, W. Zhao, H. S. Kwok and B. Z. Tang, *Chem. Commun.*, 2015, 51, 7321.

4 (a) S. W. Thomas III, G. D. Joly and T. M. Swager, *Chem. Rev.*, 2007, 107, 1339; (b) L. Basabe-Desmonts, D. N. Reinhoudt and M. Crego-Calama, *Chem. Soc. Rev.*, 2007, 36, 993; (c) A. Duarte, K.-Y. Pu, B. Liu and G. C. Bazan, *Chem. Mater.*, 2011, 23, 501.

5 (a) H. Tong, Y. Hong, Y. Dong, M. Häußler, J. W. Y. Lam, Z. Li, Z. Guo, Z. Guo and B. Z. Tang, *Chem. Commun.*, 2006, 3705; (b) Y. Hong, J. W. Y. Lam and B. Z. Tang, *Chem. Commun.*, 2009, 4332; (c) B. C. Dickinson, C. Huynh and C. J. Chang, *J. Am. Chem. Soc.*, 2010, 132, 5906; (d) W.-C. Wu, C.-Y. Chen, Y. Tian, S.-H. Jang, Y. Hong, Y. Liu, R. Hu, B. Z. Tang, Y.-T. Lee, C.-T. Chen, W.-C. Chen and A. K.-Y. Jen, *Adv. Funct. Mater.*, 2010, 20, 1413; (e) Y. Liu, Y. Yu, J. W. Y. Lam, Y. Hong, M. Faisal, W. Z. Yuan and B. Z. Tang, *Chem. Eur. J.*, 2010, 16, 8433; (f) Y. Liu, C. Deng, L. Tang, A. Qin, R. Hu, J. Z. Sun and B. Z. Tang, *J. Am. Chem. Soc.*, 2011, 133, 660; (g) D. King, K. Li, B. Liu and B. Z. Tang, *Accounts Chem. Res.*, 2013, 46, 2441; (h) K. Li, W. Qin, D. Ding, N. Tomczak, J. Geng, R. Liu, J. Liu, X. Zhang, H. Liu, B. Liu and B. Z. Tang, *Sci. Rep.*, 2013, 3; (i) D. Ding, C. C. Goh, G. Feng, Z. Zhao, J. Liu, R. Liu, N. Tomczak, J. Geng, B. Z. Tang, L. G. Ng and B. Liu, *Adv. Mater.*, 2013, 25, 6083; (j) J. Xiang, X. Cai, X. Lou, G. Feng, X. Min, W. Luo, B. He, C. C. Goh, L. G. Ng, J. Zhou, Z. Zhao, B. Liu and B. Z. Tang, *ACS Appl. Mater. Interfaces*, 2015, 7, 14965.

6 (a) W. Qin, D. Ding, J. Liu, W. Z. Yuan, Y. Hu, B. Liu and B. Z. Tang, *Adv. Funct. Mater.*, 2012, 22, 771; (b) A. Singh, C.-K. Lim, Y.-D. Lee, J.-h. Maeng, S. Lee, J. Koh and S. Kim, *ACS Appl. Mater. Interfaces*, 2013, 5, 8881; (c) F. Hu, Y. Huang, G. Zhang, R. Zhao, H. Yang and D. Zhang, *Anal. Chem.*, 2014, 86, 7987; (d) G. Liu, D. Chen, L. Kong, J. Shi, B. Tong, J. Zhi, X. Feng and Y. Dong, *Chem. Commun.*, 2015, 51, 8555.

7 (a) J. E. Raymond, G. Ramakrishna, R. J. Twieg and T. I. Goodson, *J. Phys. Chem. C*, 2008, 112, 7913; (b) V. Parthasarathy, S. Fery-Forgues, E. Campioli, G. Recher, F. Terenziani and M. Blanchard-Desce, *Small*, 2011, 7, 3219.

8 (a) Z. Xu, Q. Liao, Y. Wu, W. Ren, W. Li, L. Liu, S. Wang, Z. Gu, H. Zhang and H. Fu, *J. Mater. Chem.*, 2012, 22, 17737; (b) E. Ishow, A. Brosseau, G. Clavier, K. Nakatani, P. Tauc, C. Fiorini-Debuisschert, S. Neveu, O. Sandre and A. Léaustic, *Chem. Mater.*, 2008, 20, 6597; (c) A. D'Aléo, A. Felouat, V. Heresanu, A. Ranguis, D. Chaudanson, A. Karapetyan, M. Giorgic and F. Fages, *J. Mater. Chem. C*, 2014, 2, 5208; (d) F. He, L. Tian, X. Tian, H. Xu, Y. Wang, W. Xie, M. Hanif, J. Xia, F. Shen, B. Yang, F. Li, Y. Ma, Y. Yang and J. Shen, *Adv. Funct. Mater.*, 2007, 17, 1551; (e) Y. Jiang, Y. Wang, J. Hua, J. Tang, B. Li, S. Qian and H. Tian, *Chem. Commun.*, 2010, 46, 4689; (f) P. Liu, S. Li, Y. Jin, L. Qian, N. Gao, S. Q. Yao, F. Huang, Q.-H. Xu and Y. Cao, *ACS Appl. Mater. Interfaces*, 2015, 7, 6754−6763; (g) Y. Gao, G. Feng, T. Jiang, C. Goh, L. Ng, B. Liu, B. Li, L. Yang, J. Hua and H. Tian, *Adv. Funct. Mater.*, 2015, 25, 2857; (h) S. Kim, Q. Zheng, G. S. He, D. J. Bharali, H. E. Pudavar, A. Baev and P. N. Prasad, *Adv. Funct. Mater.*, 2007, 16, 2317; (i) S. Kim, H. E. Pudavar, A. Bonoiu and P. N. Prasad, *Adv. Mater.*, 2007, 19, 3791; (j) S. Kim, T. Y. Ohulchanskyy, H. E. Pudavar, R. K. Pandey and P. N. Prasad, *J. Am. Chem. Soc.*, 2007, 129, 2669; (k) S. Kim, H. Huang, H. E. Pudavar, Y. Cui and P. N. Prasad, *Chem. Mater.*, 2007, 19, 5650.

9 (a) F. Treussart, E. Botzung-Appert, N.-T. Ha-Duong, A. Ibanez, J.-F. Roch and R. Pansu, *ChemPhysChem*, 2003, 4, 757; (b) M. Rodríguez, G. Ramos-Ortíz, M. I. Alcalá-Salas, J. L. Maldonado, K. A. López-Varela, Y. López, O. Domínguez, M. A. Meneses-Nava, O. Barbosa-García, R. Santillan and N. Farfán, *Dyes Pigm.*, 2010, 87, 76.

10 G. Qian and Z. Y. Wang, *Chem. Asian J.*, 2010, 5, 1006.

11 M.-J. Lin, Á. J. Jiménez, C. Burschka and F. Würthner, *Chem. Commun.*, 2012, 48, 12050.

12 M. Matsui, Y. Ando, O. Tokura, Y. Kubota and K. Funabiki, *Tetrahedron*, 2013, 69, 3410.

13 (a) Y. Ooyama, S. Yoshikawa, S. Watanabe and K. Yoshida, *Org. Biomol. Chem.*, 2006, 4, 3406; (b) T. Ozdemir, S. Atilgan, I. Kutuk, S. Serdar Yildirim, A. Tulek, M. Bayindir and E. U. Akkaya, *Org. Lett.*, 2009, 11, 2105; (c) Y. Kubota, J. Uehara, K. Funabiki, M. Ebihara and M. Matsui, *Tetrahedron Lett.*, 2010, 51, 6195; (d) Y. Kubota, H. Hara, S. Tanaka, K. Funabiki and M. Matsui, *Org. Lett.*, 2011, 13, 6544; (e) H. Lu, Q. Wang, L. Gai, Z. Li, Y. Deng, X. Xiao, G. Lai and Z. Shen, *Chem. Eur. J.*, 2012, 18, 7852 ; (f) D. Li, H. Zhang, C. Wang, S. Huang, J. Guo and Y. Wang, *J. Mater. Chem.*, 2012, 22, 4319.

14 (a) Z. Fei, N. Kocher, C. J. Mohrschladt, H. Ihmels and D. Stalke, *Angew. Chem., Int. Ed.*, 2003, 42, 783; (b) Z.-F. Shi, L.-J. Wang, H. Wang, X.-P. Cao and H.-L. Zhang, *Org. Lett.*, 2007, 9, 595; (c) T. Qin, G. Zhou, H. Scheiber, R. E. Bauer, M. Baumgarten, C. E. Anson, E. J. W. List and K. Müllen, *Angew. Chem., Int. Ed.*, 2008, 47, 8292.

15 J. Mei, Y. Hong, J. W. Y. Lam, A. Qin, Y. Tang and B. Z. Tang, *Adv. Mater.*, 2014, 26, 5429.

16 (a) B.-K. An, S.-K. Kwon, S.-D. Jung and S. Y. Park, *J. Am. Chem. Soc.*, 2002, 124, 14410; (b) B.-K. An and S. Y. Park, *Functional Nanomaterials* 2006, 247; (c) J. Gierschner and S. Y. Park, *J. Mater. Chem. C*, 2013, 1, 5818.

17 (a) D. Ding, K. Li, B. Liu and B. Z. Tang, *Accounts of Chemical Research*, 2013, 46, 2441; (b) B. Z. Tang and A. Qin, *Aggregation-Induced Emission: Applications*, Wiley, 2013; (c) X. Zhang, X. Zhang, L. Tao, Z. Chi, J. Xu and Y. Wei, *J. Mater. Chem. B*, 2014, 2, 4398.

18 (a) F. D. Lewis and J.-S. Yang, *J. Phys. Chem. B*, 1997, 101, 1775; (b) Y. Ooyama, T. Okamoto, T. Yamaguchi, T. Suzuki, A. Hayashi and K. Yoshida, *Chem. Eur. J.*, 2006, 12, 7827 ; (c) R. Davis, N. S. S. Kumar, S. Abraham, C. H. Suresh, N. P. Rath, N. Tamaoki and S. Das, *J. Phys. Chem. C*, 2008, 112, 2137; (d) Z. Zhang, Y. Zhang, D. Yao, H. Bi, I. Javed, Y. Fan, H. Zhang and Y. Wang, *Cryst. Growth Des.*, 2009, 9, 5069; (e) S.-Y. Park, M. Ebihara, Y. Kubota, K. Funabiki and M. Matsui, *Dyes Pigm.*, 2009, 82, 258; (f) F. Gao, Q. Liao, Z.-Z. Xu, Y.-H. Yue, Q. Wang, H.-L. Zhang and H.-B. Fu, *Angew. Chem., Int. Ed.*, 2010, 49, 732; (g) C. Kitamura, Y. Abe, T. Ohara, A. Yoneda, T. Kawase, T. Kobayashi, H. Naito and T. Komatsu, *Chem. Eur. J.*, 2010,

16, 890; (h) M. Shimizu, R. Kaki, Y. Takeda, T. Hiyama, N. Nagai, H. Yamagishi and H. Furutani, *Angew. Chem., Int. Ed.*, 2012, 51, 4095; (i) B. Dong, M. Wang, C. Xu, Q. Feng and Y. Wang, *Cryst. Growth Des.*, 2012, 12, 5986−5993; (j) M. Santra, H. Moon, M.-H. Park, T.-W. Lee, Y. K. Kim and K. H. Ahn, *Chem. Eur. J.*, 2012, 18, 9886; (k) A. D'Aléo, D. Gachet, V. Heresanu, M. Giorgi and F. Fages, *Chem. Eur. J.*, 2012, 18, 12764; (l) L. Quan, Y. Chen, X.-J. Lv and W.-F. Fu, *Chem. Eur. J.*, 2012, 18, 14599; (m) Z. Zheng, Z. Yu, M. Yang, F. Jin, Q. Zhang, H. Zhou, J. Wu and Y. Tian, *J. Org. Chem.*, 2013, 78, 3222−3234; (n) X. Y. Shen, Y. J. Wang, E. Zhao, W. Z. Yuan, Y. Liu, P. Lu, A. Qin, Y. Ma, J. Z. Sun and B. Z. Tang, *J. Phys. Chem. C*, 2013, 117, 7334−7347.

19 B. Kupcewicz and M. Małecka, *Cryst. Growth Des.*, 2015, 15, 3893.

20 (a) J. Massin, W. Dayoub, J.-C. Mulatier, C. Aronica, Y. Bretonnière and C. Andraud, *Chem. Mater.*, 2011, 23, 862; (b) Z. Zhang, R. M. Edkins, J. Nitsch, K. Fucke, A. Eichhorn, A. Steffen, Y. Wang and T. B. Marder, *Chem. Eur. J.*, 2015, 21, 177.

21 (a) C. Zhang, L. R. Dalton, M.-C. Oh, H. Zhang and W. H. Steier, *Chem. Mater.*, 2001, 13, 3043; (b) W. Bentoumi, J.-C. Mulatier, P.-A. Bouit, O. Maury, A. Barsella, J.-P. Vola, E. Chastaing, L. Divay, F. Soyer, P. Le Barny, Y. Bretonnière and C. Andraud, *Chem. Eur. J.*, 2014, 20, 8909.

22 (a) S. J. Lord, Z. Lu, H. Wang, K. A. Willets, P. J. Schuck, H.-l. D. Lee, S. Y. Nishimura, R. J. Twieg and W. E. Moerner, *The journal of physical chemistry. A*, 2007, 111, 8934; (b) S. J. Lord, N. R. Conley, H.-l. D. Lee, S. Y. Nishimura, A. K. Pomerantz, K. A. Willets, Z. Lu, H. Wang, N. Liu, R. Samuel, R. Weber, A. Semyonov, M. He, R. J. Twieg and W. E. Moerner, *ChemPhysChem*, 2009, 10, 55; (c) H. Wang, Z. Lu, S. J. Lord, K. A. Willets, J. A. Bertke, S. D. Bunge, W. E. Moerner and R. J. Twieg, *Tetrahedron*, 2007, 63, 103; (d) H.-l. D. Lee, S. J. Lord, S. Iwanaga, K. Zhan, H. Xie, J. C. Williams, H. Wang, G. R. Bowman, E. D. Goley, L. Shapiro, R. J. Twieg, J. Rao and W. E. Moerner, *J. Am. Chem. Soc.*, 2010, 132, 15099; (e) Y. Jin, Y. Tian, W. Zhang, S.-H. Jang, A. K.-Y. Jen and D. R. Meldrum, *Anal. Bioanal. Chem.*, 2010, 398, 1375; (f) H. Y. Yoon, S. H. Shim, L. J. Baek and J.-I. Hong, *Bioorg. Med. Chem. Lett.*, 2011, 21, 2403; (g) X. Zhou, F. Su, Y. Tian, C. Youngbull, R. H. Johnson and D. R. Meldrum, *J. Am. Chem. Soc.*, 2011, 133, 18530; (h) M.-Y. Wu, K. Li, C.-Y. Li, J.-T. Hou and X.-Q. Yu, *Chem. Commun.*, 2014, 50, 183.

23 L. Feng, Z.-M. Liu, L. Xu, X. Lv, J. Ning, J. Hou, G.-B. Ge, J.-N. Cui and L. Yang, *Chem. Commun.*, 2014, 50, 14519.

24 (a) E. Font-Sanchis, F. J. Céspedes-Guirao, Á. Sastre-Santos, B. Villacampa, J. Orduna, R. Alicante and F. Fernández-Lázaro, *Tetrahedron*, 2009, 65, 4513; (b) E. Font-Sanchis, R. E. Galian, F. J. Céspedes-Guirao, Á. Sastre-Santos, L. R. Domingo, F. Fernández-Lázaro and J. Pérez-Prieto, *Phys. Chem. Chem. Phys.*, 2010, 12, 7768; (c) F. Gallego-Gómez, J. C. Álvarez-Santos, J. L. Rodríguez-Redondo, E. Font-Sanchis, J. M. Villalvilla, Á. Sastre-Santos, M. A. Díaz-García and F. Fernández-Lázaro, *J. Mater. Chem.*, 2012, 22, 12220.

25 G. Koeckelberghs, S. Sioncke, T. Verbiest, A. Persoons and C. Samyn, *Polymer*, 2003, 44, 3785.

26 CrysAlisPro, Agilent Technologies, Version 1.171.35.21 (release 20-01-2012 CrysAlis171 .NET) (compiled Jan 23 2012,18:06:46)

27 R. C. Clark and J. S. Reid, *Acta Crystallogr.*, 1995, A51, 887.

28 A. Altomare, M. C. Burla, M. Camalli, G. L. Cascarano, C. Giacovazzo, A. Guagliardi, A. G. G. Moliterni, G. Polidori and R. Spagna, *J. Appl. Crystallogr.*, 1999, 32, 115.

29 P. W. Betteridge, J. R. Carruthers, R. I. Cooper, K. Prout and D. J. Watkin, *J. Appl. Crystallogr.*, 2003, 36, 1487.

30 J. R. Lakowicz, in *Principle of Fluorescene Spectroscopy*, ed. K. Academic/Plenum, New York, 3rd edn., 2006, pp. 873.

31 J. C. de Mello, H. F. Wittmann and R. H. Friend, *Adv. Mater.*, 1997, 9, 230.

32 L. Porrès, A. Holland, L.-O. Pålsson, A. P. Monkman, C. Kemp and A. Beeby, *J. Fluoresc.*, 2006, 16, 267.

33 (a) D. Villemin and L. Liao, *Synth. Commun.*, 2001, 31, 1771; (b) S. Liu, M. A. Haller, H. Ma, L. R. Dalton, S.-H. Jang and A. K.-Y. Jen, *Adv. Mater.*, 2003, 15, 603.

34 H. Kasai, H. Singh Nalwa, S. Okada, H. Oikawa and H. Nakanishi, in *Handbook of Nanostructured Materials and Nanotechnology*, ed. H. S. Nalwa, Academic Press, Burlington, 2000, pp. 433.

35 (a) S. Kim, Q. Zheng, G. S. He, D. J. Bharali, H. E. Pudavar, A. Baev and P. N. Prasad, *Adv. Funct. Mater.*, 2006, 16, 2317; (b) X. Zhang, Z. Chi, B. Xu, H. Li, Z. Yang, X. Li, S. Liu, Y. Zhang and J. Xu, *Dyes Pigm.*, 2011, 89, 56; (c) X. Zhang, Z. Chi, B. Xu, C. Chen, X. Zhou, Y. Zhang, S. Liu and J. Xu, *J. Mater. Chem.*, 2012, 22, 18505.

36 D. Li, K. Wang, S. Huang, S. Qu, X. Liu, Q. Zhu, H. Zhang and Y. Wang, *J. Mater. Chem.*, 2011, 21, 15298.

37 J.-H. Olivier, J. Widmaier and R. Ziessel, *Chem. Eur. J.*, 2011, 11709.

38 (a) C. Kitamura, Y. Abe, N. Kawatsuki, A. Yoneda, K. Asada, T. Kobayashi and H. Naito, *Mol. Cryst. Liq. Cryst.*, 2007, 414, 119; (b) N. S. S. Kumar, S. Varghese, C. H. Suresh, N. P. Rath and S. Das, *J. Phys. Chem. C*, 2009, 113, 11927; (c) L. Fan, Q. Liu, D. Lu, H. Shi, Y. Yang, Y. Li, C. Dong and S. Shuang, *J. Mater. Chem. B*, 2013, 1, 4281; (d) C. Spies, A.-M. Huynh, V. Huch and G. Jung, *J. Phys. Chem. C*, 2013, 117, 18163.

39 (a) O.-P. Kwon, B. Ruiz, A. Choubey, L. Mutter, A. Schneider, M. Jazbinsek, V. Gramlich and P. Günter, *Chem. Mater.*, 2006, 18, 4049; (b) S. Li, M. Li, J. Qin, M. Tong, X. Chen, T. Liu, Y. Fu, S. Wu and Z. Su, *CrystEngComm*, 2009, 11; (c) J. Kim, J.-Y. Seo, M. Jazbinsek, S.-J. Kwon, E.-Y. Choi, J.-I. Seo, H. Yun, Y. S. Lee, P. Günter and O.-P. Kwon, *J. Phys. Chem. C*, 2012, 116, 25034; (d) G. J. Gainsford, M. Ashraf and A. J. Kay, *Acta Crystallogr. E*, 2012, E68, o2991.

40 F. Würthner, T. E. Kaiser and C. R. Saha-Müller, *Angew. Chem., Int. Ed.*, 2011, 50, 3376

41 (a) X. Wang, A. R. Morales, T. Urakami, L. Zhang, M. V. Bondar, M. Komatsu and K. D. Belfield, *Bioconjugate Chem.*, 2011, 22, 1438; (b) M. Breton, G. Prével, J.-F. Audibert, R. Pansu, P. Tauc, B. Le Pioufle, O. Français, J. Fresnais, J.-F. Berrete and E. Ishow, *Phys. Chem. Chem. Phys.*, 2011, 13, 13268.

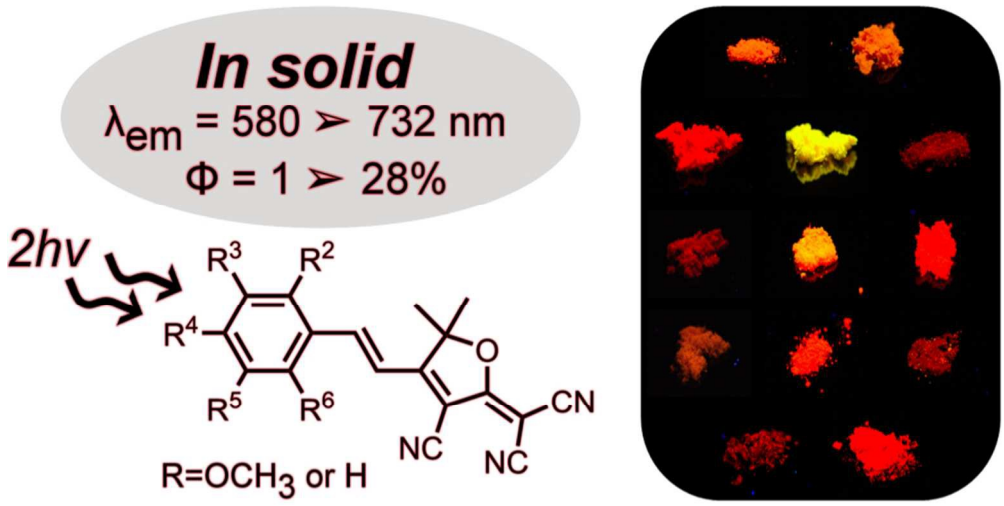

80x39mm (300 x 300 DPI)